Journal of Cellular Physiology

Transcriptome-based screening of ion channels and transporters in a migratory chondroprogenitor cell line isolated from late-stage osteoarthritic cartilage

Journal:	*Journal of Cellular Physiology*
Manuscript ID	JCP-20-4421.R2
Wiley - Manuscript type:	Original Research Article
Date Submitted by the Author:	n/a
Complete List of Authors:	Matta, Csaba; University of Debrecen, Department of Anatomy, Histology and Embryology; University of Surrey Lewis, Rebecca; University of Surrey Fellows, Christopher; University of Surrey Diszhazi, Gyula; University of Debrecen, Department of Physiology Almassy, Janos; University of Debrecen, Department of Physiology Miosge, Nicolai; Georg-August-Universitat Gottingen, Department of Prosthodontics Dixon, James; University of Nottingham, Centre of Biomolecular Sciences Uribe, Marcos; University of Nottingham, The Nottingham Arabidopsis Stock Centre (NASC), School of Biosciences May, Sean; University of Nottingham, The Nottingham Arabidopsis Stock Centre (NASC), School of Biosciences Poliska, Szilard; University of Debrecen, Genomic Medicine and Bioinformatic Core Facility, Department of Biochemistry and Molecular Biology Barrett-Jolley, Richard; University of Liverpool Faculty of Health and Life Sciences, Institute of Ageing and Chronic Disease Fodor, Janos; University of Debrecen, Department of Physiology Szentesi, Peter; University of Debrecen, Department of Physiology Hajdu, Tibor; University of Debrecen, Department of Anatomy, Histology and Embryology Keller-Pinter, Aniko; University of Szeged Faculty of Medicine, Department of Biochemistry Henslee, Erin; University of Surrey, Centre for Biomedical Engineering, Department of Mechanical Engineering Sciences Labeed, Fatima; University of Surrey, Centre for Biomedical Engineering, Department of Mechanical Engineering Sciences Hughes, Michael; University of Surrey, Centre for Biomedical Engineering, Department of Mechanical Engineering Sciences Mobasheri, Ali; University of Oulu, Research Unit of Medical Imaging, Physics and Technology, Faculty of Medicine; State Research Institute Centre for Innovative Medicine, Department of Regenerative Medicine; University Medical Center Utrecht, 13Departments of Orthopedics, Rheumatology and Clinical Immunology; Sun Yat-sen University First Affiliated Hospital, Department of Joint Surgery
Key Words:	Mesenchymal stem cell, Osteoarthritis, Chondroprogenitor,

	Transcriptomics, Channelome

Revised Manuscript - JCP-20-4421R2

Transcriptome-based screening of ion channels and transporters in a migratory chondroprogenitor cell line isolated from late-stage osteoarthritic cartilage

Csaba Matta[1,2,*,$], Rebecca Lewis[2,*], Christopher Fellows[2], Gyula Diszhazi[3], Janos Almassy[3], Nicolai Miosge[4], James Dixon[5], Marcos C. Uribe[6], Sean May[6], Szilard Poliska[7], Richard Barrett-Jolley[8], Janos Fodor[3], Peter Szentesi[3], Tibor Hajdú[1], Aniko Keller-Pinter[9], Erin Henslee[10], Fatima H. Labeed[10], Michael P. Hughes[10], Ali Mobasheri[11,12,13,14,$]

[1]*Department of Anatomy, Histology and Embryology, Faculty of Medicine, University of Debrecen, Debrecen, H-4032, Hungary*

[2]*Department of Veterinary Preclinical Sciences, School of Veterinary Medicine, Faculty of Health and Medical Sciences, University of Surrey, Guildford, Surrey, GU2 7AL, United Kingdom*

[3]*Department of Physiology, Faculty of Medicine, University of Debrecen, Debrecen, H-4032, Hungary*

[4]*Department of Prosthodontics, Tissue Regeneration Work Group, Georg August University, Göttingen, Germany*

[5]*School of Pharmacy, Wolfson Centre for Stem Cells, Tissue Engineering, and Modelling, Centre of Biomolecular Sciences, University of Nottingham, Nottingham, NG7 2RD, United Kingdom*

[6]*The Nottingham Arabidopsis Stock Centre (NASC), School of Biosciences, University of Nottingham, Sutton Bonington Campus, Loughborough, LE12 5RD, United Kingdom*

[7]*Genomic Medicine and Bioinformatic Core Facility, Department of Biochemistry and Molecular Biology, Faculty of Medicine, University of Debrecen, Debrecen, H-4032, Hungary*

[8]*Department of Musculoskeletal Biology, Faculty of Health and Life Sciences, Institute of Ageing and Chronic Disease, University of Liverpool, Liverpool, L69 3GA, United Kingdom*

[9]*Department of Biochemistry, Faculty of Medicine, University of Szeged, H-6720 Szeged, Hungary*

[10]*Centre for Biomedical Engineering, Department of Mechanical Engineering Sciences, University of Surrey, Guildford, Surrey GU2 7XH, UK*

[11]*Department of Regenerative Medicine, State Research Institute Centre for Innovative Medicine, Vilnius, Lithuania*

[12]*Research Unit of Medical Imaging, Physics and Technology, Faculty of Medicine, University of Oulu, FIN-90230 Oulu, Finland*

[13]*Departments of Orthopedics, Rheumatology and Clinical Immunology, University Medical Center Utrecht, 3584 CX Utrecht, The Netherlands*

[14]*Department of Joint Surgery, the First Affiliated Hospital, Sun Yat-sen University, Guangzhou 510080, China*

*C.M. and R.L. should be considered joint first author.

[$]Corresponding authors: Csaba Matta – e-mail: matta.csaba@med.unideb.hu

Ali Mobasheri – e-mail: ali.mobasheri@oulu.fi

Running title: Ion channels in chondroprogenitor cells

Abstract

Chondrogenic progenitor cells (CPCs) may be used as an alternative source of cells with potentially superior chondrogenic potential compared to mesenchymal stem cells (MSCs), and could be exploited for future regenerative therapies targeting articular cartilage in degenerative diseases such as osteoarthritis (OA). In this study, we hypothesised that CPCs derived from OA cartilage may be characterised by a distinct channelome. First, a global transcriptomic analysis using Affymetrix microarrays was performed. We studied the profiles of those ion channel and transporter families that may be relevant to chondroprogenitor cell physiology. Following validation of the microarray data with qRT-PCR, we examined the role of calcium-dependent potassium channels in CPCs and observed functional large conductance calcium-activated potassium (BK) channels involved in the maintenance of the chondroprogenitor phenotype. In line with our very recent results, we found that the KCNMA1 gene was upregulated in CPCs and observed currents that could be attributed to the BK channel. The BK channel inhibitor paxilline significantly inhibited proliferation, increased the expression of the osteogenic transcription factor RUNX2, enhanced the migration parameters, and completely abolished spontaneous Ca^{2+} events in CPCs. Through characterisation of their channelome we demonstrate that CPCs are a distinct cell population but are highly similar to MSCs in many respects. This work adds key mechanistic data to the in-depth characterisation of CPCs and their phenotype in the context of cartilage regeneration.

(225 words in abstract)

Keywords

Chondrocyte; Cartilage; Mesenchymal stem cell; Osteoarthritis; Chondroprogenitor; Transcriptomics; Channelome

List of abbreviations

AD-MSC, adipose tissue-derived mesenchymal stem cell; BK; large conductance calcium-activated potassium channel; BM-MSC, marrow-derived mesenchymal stem cell; CPC, chondrogenic progenitor cell; CRAC; Ca^{2+} release-activated Ca^{2+} channel; DEP, dielectrophoresis; ECM, extracellular matrix; ENaC; epithelial sodium channel; GAG, glycosaminoglycan; IBTX, iberiotoxin; MSC, mesenchymal stem cell; OA, osteoarthritis; PCA, principal component analysis; PG, proteoglycan; RMP, resting membrane potential; SOCE, store-operated Ca^{2+} entry; TRP, transient receptor potential

Introduction

The prevalence of musculoskeletal conditions is constantly increasing, making age-related and chronic inflammatory joint diseases the major causes of disability in the elderly population (Al Maini et al., 2020). Osteoarthritis (OA) is the most common form of chronic musculoskeletal disorders (Hunter & Bierma-Zeinstra, 2019). Although the primary target of OA is articular cartilage, it also affects other tissues within and around the joint (Loeser et al., 2012). The affected tissues undergo metabolic, structural and functional alterations that contribute to joint pain, disease progression, and patient disability (Henrotin et al., 2016).

Chondrocytes are the main cell type in articular cartilage (Archer & Francis-West, 2003), along with a scarce population of cartilage progenitor cells (CPCs) (Nakayama et al., 2020). The resident cells are embedded in a cartilage-specific extracellular matrix (ECM) that consists of collagen type II, large aggregating proteoglycans (PG; e.g. aggrecan), constituent glycosaminoglycans (GAG), hyaluronan, small PGs, and other collagenous and non-collagenous proteins (Buckwalter et al., 2005). A high amount of interstitial water (approximately 80% of total weight of cartilage) is osmotically drawn to the freely mobile cations (i.e. Na^+, K^+, Ca^{2+}) balancing the negatively charged GAG side chains of PGs and are therefore present at high local concentrations. Cells in cartilage ECM are thus exposed to a unique ionic micro-environment (Mobasheri et al., 1998; Urban et al., 1993). Cartilage is avascular, and as a consequence of the scarcity of available nutrients and oxygen, its unique, relatively hypoxic and acidic milieu, as well as low cellularity, it is incapable of mounting a sufficient healing and repair response following injury (Gomoll & Minas, 2014).

The presence of a cartilage-specific CPC population with stem cell properties in the superficial zone of articular normal cartilage is now widely accepted (Dowthwaite et al., 2004). More recently, cells in OA articular cartilage with mesenchymal progenitor cell characteristics have also been observed and characterised (Fellows et al., 2017). These cartilage

progenitor/stem cell populations have the potential for chondrogenic induction and tri-lineage plasticity. CPCs have also been described in late-stage OA cartilage, which are believed to be migrating in response to chemotactic signals from the bone marrow through breaks in the tide mark, as an attempt to regenerate damaged cartilage ECM (Koelling et al., 2009). However, knowledge concerning the specific phenotypic features and regenerative potentials of chondroprogenitor cells is still incomplete. CPCs are considered an ideal source for cell-based cartilage repair, and therefore progress has been made in identifying, understanding, and characterizing these cells.

In OA, chondrocytes and CPCs exist in a micro-environment dominated by mediators that promote matrix degradation and low-grade inflammation. There is evidence that cartilage ECM undergoes profound alterations during OA in terms of GAG and water content (Mankin & Lippiello, 1970). That in turn alters the osmolality of the matrix and the composition of the unique ionic milieu (Mow et al., 1999). Chondrocytes and other cells in cartilage respond to these changes and maintain their homeostasis by altering the transport of ions across the cell membrane (Hdud et al., 2014) via transporters and ion channels, collectively referred to as the 'channelome' (Asmar et al., 2016; Barrett-Jolley et al., 2010; Mobasheri et al., 2019).

Plasma membrane transporters including voltage-gated sodium, potassium and calcium channels, chloride channels, calcium-activated potassium channels, transient receptor potential (TRP) channels, N-methyl-D-aspartate (NMDA) receptors and purinergic receptors have been described in chondrocytes, which allow them to respond to the local ionic composition of the pericellular matrix by adjusting the resting membrane potential (RMP) (Maleckar et al., 2020), which has been shown to play a crucial role in regulating metabolic activity and synthetic rate of cartilage ECM, as well as proliferation, differentiation, or volume regulation (Asmar et al., 2016; Matta & Zakany, 2013; Mobasheri et al., 2019). Although much progress has been made towards characterising the chondrocyte channelome, many open questions remain concerning

the composition of the ion channel complement and their function in chondroprogenitor cells. Whilst there is accumulating data suggesting that several genes encoding ion channels which are involved in the regulation of mechanotransduction, cell volume, RMP, and apoptosis are differentially expressed in OA chondrocytes (Lewis & Barrett-Jolley, 2015), current understanding concerning the channelome of CPCs, especially with regards to differentially regulated ion channel genes, is incomplete. Addressing this gap in knowledge is high priority for identification and targeting of new therapeutic targets for the treatment of OA.

In this study we hypothesised that CPCs derived from OA cartilage may be characterised by a different assembly of ion channels and transporters that regulate their function and phenotype, and maintain communication with the altered ECM. Given that there is some evidence that migratory CPCs are related to MSCs residing in the bone marrow close to the subchondral bone which have migrated to lesioned cartilage through breaks in the tide mark, we used bone marrow-derived MSCs (BM-MSCs) as a reference cell population. We have recently analysed the surfaceome of CPCs using selective cell surface protein labelling followed by quantitative high-throughput mass spectrometry and identified alterations in the composition of the surfaceome compared to MSCs (Matta et al., 2019). However, even that approach was not sensitive enough to detect alterations in very low-abundance ion channels or other transporters. In this study, we attempted to differentiate CPCs from BM-MSCs based on their transcriptome and electrophysiological properties. We first performed a global transcriptomic analysis using Affymetrix microarrays. We studied the profiles of those ion channel and transporter families that are known to be involved in regulating chondrocyte physiology, RMP, volume regulation, calcium signalling, matrix secretion, or chondrogenesis, which may have a relevance in chondroprogenitor cell physiology (Barrett-Jolley et al., 2010; Matta & Zakany, 2013; Mobasheri et al., 2019; Suzuki et al., 2020). We then employed patch clamping and dielectrophoresis to characterise the basic electrophysiological profile (the

'electrome' (De Loof, 2016)) of the two cell types. Following validation of the microarray data using RT-qPCR, we examined the role of calcium-dependent potassium channels in the cellular physiology and homeostasis of migratory CPCs and found that the large conductance calcium-activated potassium channels (BK) are functionally expressed and are involved in the maintenance of the chondroprogenitor phenotype.

Materials and methods

1. Cell culture

Experiments were carried out on a human migratory CPC cell line derived from late-stage OA knee articular cartilage, which has been immortalised by viral transfection of the human telomerase reverse transcriptase (hTERT) as previously described (Koelling et al., 2009). CPCs were cultured in monolayers in 75 cm^2 cell culture flasks (Nunc, Thermo Fisher Scientific, Waltham, MA, USA) until ~80% confluence in GlutaMax DMEM (1.0 g/L glucose; Gibco, Thermo Fisher Scientific) containing 10% FCS (foetal calf serum; Gibco) and 50 µg/mL gentamycin (Sigma-Aldrich, St. Louis, MO, USA). As a reference cell population, human BM-MSCs (Lonza, Basel, Switzerland) were used. The cells were received at passage 2 and were expanded until passage 4 in Lonza hMSC medium at 37°C in a humidified atmosphere of 5% CO_2. MSCs were hTERT-immortalised as previously described in (Okamoto et al., 2002) with the modifications detailed in (Saeed et al., 2015). Immortalised MSCs were expanded in monolayers in 75 cm^2 cell culture flasks (Nunc) until ~80% confluence in GlutaMax DMEM (4.5 g/L glucose; Gibco) containing 10% FCS (Gibco) and 1% P/S (Sigma-Aldrich).

2. RNA isolation and reverse transcription

Total RNA was isolated from cells grown in monolayers in 75 cm^2 cell culture flasks using the RNeasy kit (Qiagen, Hilden, Germany) as per the instructions of the manufacturer, and stored at –80°C. RNA concentration and purity was determined by a Nanodrop 2000 UV-Vis spectrophotometer (Thermo Fisher Scientific). For gene expression analyses, 2 µg of RNA was reverse transcribed into complementary cDNA using the High-Capacity cDNA Reverse Transcription Kit (Thermo Fisher Scientific), following the protocol supplied by the manufacturer. cDNA was stored at –20°C.

3. Affymetrix microarray analysis

RNA integrity was confirmed using an Agilent 2100 Bioanalyzer with the RNA 6000 Nano Kit (Agilent Technologies, Palo Alto, CA). The RNA integrity numbers (RIN) were ≥ 9.6 for all samples. Whole-genome transcriptome analysis was conducted by hybridising three biological samples of total RNA per cell type to Affymetrix Human Gene 2.1 ST Arrays Strips (Affymetrix, Santa Clara, CA, USA). All steps were conducted at the Nottingham Arabidopsis Stock Centre. Gene expression data were analysed using Partek Genomics Suite 6.6 software (Partek Incorporated, St. Louis, MO, USA). The raw CEL files were normalised using the RMA background correction with quantile normalisation, log base 2 transformation and mean probe-set summarisation with adjustment for GC content. Differentially expressed genes (DEG) were identified by a two-way ANOVA, and *P*-values were adjusted using the false-discovery rate (FDR) method to correct for multiple comparisons. DEG were considered significant if *P*-value with FDR was ≤ 0.05. The expression data of genes coding for selected transporter and ion channel subunits are summarised in Tables S1–S4 in the Supporting Information. The data set is published in a MIAME compliant format in the GEO database

(http://www.ncbi.nlm.nih.gov/geo/); accession numbers: GSM4885525-GSM4485530 (GSE160886). **Reviewer token: chanoygyjbudnun**

4. Pathway analysis

CytoScape v3.4 software with ClueGo v2.3.5 application was used for identifying over-represented Gene ontology (GO) terms. Two-sided hypergeometric test with Bonferroni step down correction was performed using the list of differentially expressed genes and the GO Biological process database.

5. Quantitative real-time polymerase chain reaction (RT-qPCR) analyses

Selected ion channel subunit genes were analysed by RT-qPCR using a custom configured TaqMan 96-Well Fast Gene Expression Array plate (see Tables S5–S6 in the Supporting Information) and then by absolute quantification using the standard curve method. Primer pairs were ordered from Eurogentec (Liège, Belgium). For sequences of primer pairs please see Table S7 in the Supporting Information. First, standard curves had been generated by conventional PCR using the Promega GoTaq Flexi DNA Polymerase kit (Promega, Madison, WI, USA) by adding the following components (per 50 µL reaction): 1.25 U GoTaq polymerase; 3 mM $MgCl_2$; 0.2 mM dNTP; 200 nM primers; and 10 ng cDNA. Amplification was performed in a Techne Prime Thermal Cycler (Techne, Bibby Scientific Ltd, Stone, UK) using the following thermal profile: initial denaturation at 95°C for 5 minutes, followed by 40 cycles of denaturation at 95°C for 15 sec, annealing at 58°C for 20 sec, extension at 74°C for 20 sec, and then final extension at 74°C for 5 minutes. PCR products were isolated using a Roche High Pure PCR Product Purification Kit (Roche, Basel, Switzerland) according to the instructions of the manufacturer. DNA concentration of purified PCR products was determined

using a Nanodrop 2000 UV-Vis spectrophotometer (Thermo Fisher Scientific). Standard curves were prepared by a serial (10-fold) dilution starting from 1 ng/µL.

RT-qPCR reactions were set up using the Promega GoTaq qPCR Master Mix and 20 ng input cDNA per each 10-µL reaction. Reactions were run in a Techne Prime Pro 48 Real-time qPCR machine using the following thermal profile: activation and initial denaturation at 95°C for 10 minutes, followed by 40 cycles of denaturation at 95°C for 10 sec, annealing at 58°C for 30 sec, extension at 72°C for 20 sec, and then final extension at 72°C for 20 sec. Due to spatial limitations in the 48-well qPCR plates, quantification of qPCR products was performed by absolute quantification using the standards prepared in the previous step, followed by normalising the expressional data of genes of interest to those of the most stably expressed reference gene (*PPIA*), and then the expression levels for the genes were normalised to those in MSCs (set at 1.0). The optimal normalization gene was selected using the NormFinder algorithm (Andersen et al., 2004). RT-qPCR reactions were performed on 3 biological replicates ($N = 3$).

6. Cell proliferation and mitochondrial activity assays

To assess the effect of BK channel modulators, cells were plated into 96-well plates at a density of 5,000 cells/well. Prior to the assays, cells were incubated for 48 h in the presence of the selective BK channel blocker iberiotoxin (100 nM; Tocris, Bio-Techne, Minneapolis, MN, USA); the potent BK channel inhibitor paxilline (1 µM); the BK channel activator NS1619 (10 µM; Sigma-Andrich); or vehicles at equal volumes (water, DMSO and ethanol, respectively). Rate of cell proliferation was determined by detecting the amount of incorporated radioactivity from ^{3}H-thymidine. 1 µCi/mL ^{3}H-thymidine (diluted from methyl-^{3}H-thymidine; 185 GBq/mM, Amersham Biosciences, Budapest, Hungary) was added to each well (Wallac, PerkinElmer Life and Analytical Sciences, Shelton, CT, USA) for 24 h. After washing with

PBS, proteins were precipitated with ice-cold 5% trichloroacetic acid, and rinsed with PBS again. Cells were then air-dried and radioactivity was counted by a liquid scintillation counter (Chameleon, Hidex, Turku, Finland). Measurements were carried out in 7 samples of each experimental group (n = 7) in 3 independent experiments (N = 3). For mitochondrial activity assays, 10 µL MTT reagent (thiazolyl blue tetrazolium bromide; 5 mg MTT/mL PBS; Sigma-Aldrich) was pipetted into each well. Cells were incubated for 2 h at 37°C, and following the addition of 500 µL MTT solubilizing solution, optical density was measured at 570 nm (Chameleon, Hidex).

7. Migration assays

7.1. Boyden chemotaxis chamber

CPCs were washed twice in PBS, harvested with 0.25% trypsin (Sigma-Aldrich) and resuspended in culture medium. The lower wells of a 48-well Boyden chemotaxis chamber (Neuro Probe Inc., Gaithersburg, MD, USA) were filled with 1 µL/mL human fibronectin (Sigma-Aldrich) dissolved in PBS, and covered with a polycarbonate filter (Neuro Probe Inc.) containing pores with a diameter of 3 µm. Cell suspension (50 µL) at a density of 2×10^5 cells/mL was inoculated into the wells on the top of the membrane and the chamber was incubated for 5 h at 37°C in a humidified atmosphere with or without 1 µM paxilline. Non-migrated cells were removed from the cis surface of the membrane and after fixation in methanol, migrated cells were stained with 1% toluidine blue (Sigma-Aldrich) dissolved in water. Membranes were air-dried and mounted with Pertex medium (Sigma-Aldrich). Toluidine blue-stained migratory cells were counted on the trans surface of the membrane by an internally developed MATLAB (Mathworks Inc., Natick, MA, USA) application. Cells were defined by an approximate range of values in the RGB colour space with a particle size of at least 30 pixels. Other structures, primarily membrane pores, cell debris and staining

artefacts, were omitted based on their different overall size and their distinct position in the RGB colour space. Cells in six wells were counted in each experimental group and three independent assays ($N = 3$) were performed.

7.2. Time-Lapse Imaging of Live Cells

Live-cell imaging was carried out using the CytoSMART 2 imaging system (CytoSMART Technologies, Eindhoven, Netherlands). For imaging, cells were seeded in 35-mm petri dishes at a density of 1×10^4 cells. After allowing the cells to adhere for 120 min, the petri dishes were transferred onto the device and imaging has started, either with or without 1 µM paxilline. Phase contrast time-lapse images were obtained automatically at 30 min intervals for 18 h at 37°C and 5% CO_2. Time-lapse images were analysed using ImageJ (National Institutes of Health, Bethesda, MD, USA, https://imagej.nih.gov/ij/) and CellTracker (http://celltracker.website/) software programs. The cells were tracked manually through every frame, and the x and y coordinates of the movements were recorded. We excluded dying, dividing, or damaged cells from the analysis. The length of total path, maximal distance from origin, as well as the average and maximum cell speeds were calculated. To create wind rose plots illustrating the trajectories, the migratory tracks of the individual cells were shifted to a common origin. Three independent experiments ($N = 3$) were performed.

8. Electrophysiology

8.1. Dielectrophoresis (DEP)

Cells were grown to ~80% confluence before analysis. Cells were dissociated from the culture plates by trypsinisation. Afterwards, cells were washed twice and resuspended in an iso-osmotic DEP medium with low ionic strength containing 8.5% (*w/v*) sucrose (Sigma-Aldrich, St. Louis, MO, USA), 0.3% (*w/v*) glucose (Sigma-Aldrich), and adjusted to a final

conductivity of 10 mS/m using phosphate buffered saline (PBS; Sigma-Aldrich). Buffer conductivity was measured with a conductivity meter (RS Components Ltd, London, UK). Cell counts and viability for each experiment were determined using a haemocytometer and trypan blue, which indicated a 96% ± 2% viability. To reduce the effect of variation in cell numbers in each sample, the final cell concentration was adjusted to 5×10^5 cells/mL.

DEP spectra were obtained using the 3DEP DEP-Well system (Deptech, Guildford, UK), as described in more detail earlier (Labeed et al., 2011). Briefly, cells resuspended in DEP media were administered into the wells of DEP-Well chips containing 12 ring-shaped, 17 µm wide, gold-plated copper electrodes around the well circumference with gaps of 75 µm between electrodes, and energised with currents at specific frequencies. The DEP method is based on the principle that the cells are either attracted or repelled from the side of the well by an amount proportional to their polarizability, as described previously (Hoettges et al., 2019).

Changes in light intensity across the wells over time were determined using a 1.3 Mpixel video camera installed on the microscope and a MATLAB (Mathworks Inc.) script. The change in cell distribution was monitored by recording an image every 3 s for a total of 30 s. The entire well was divided into 10 segments that were monitored separately; however, only segments 7–9 were analysed as previously described (Hoettges et al., 2008). The wells were energised with frequencies ranging from 1 kHz–20 MHz at 5 points per decade. Spectra were generated using MATLAB (Mathworks Inc.), and presented in values of light intensity versus frequency. Light intensity data were fit to the single shell model (Broche et al., 2005) and the best-fit model was used to determine the following features: specific membrane capacitance (C_{spec}), specific membrane conductance (G_{spec}), and crossover frequency (i.e. the frequency where the DEP force is zero). The best-fit model (highest Pearson correlation coefficient) was established by matching the curve to the measured data and adjusting the dielectric cytoplasmic and membrane parameters until the best match was found. MATLAB scripts were used for all

images as well as for signal processing and data analysis as previously described (Hoettges et al., 2008). Given that the key parts of the DEP curve (starting and end values and transition frequencies) can be associated with the membrane capacitance and conductance, and cytoplasm conductivity and permittivity, these parameters were determined uniquely by fitting the curve to the data points. Cell diameters were measured in a haemocytometer and the average radius was calculated using ImageJ software version 1.51 (http://imagej.nih.gov/ij/); the mean radii were used for the DEP model. All experiments were repeated three times (N = 3 independent experiments); data are expressed as mean ± standard deviation (SD).

8.2. Patch clamp

Whole cell currents were measured under voltage clamp conditions as described earlier (Almassy & Begenisich, 2012). Extracellular solution contained (in mM): NaCl, 140; KCl, 5; $CaCl_2$, 2; $MgCl_2$, 1; HEPES, 10; glucose, 5; pH 7.4 with NaOH. Patch pipettes were fabricated from thick-walled borosilicate glass (o.d. 1.5 mm, i.d. 0.85 mm) with resistance of approximately 5 MΩ when filled with intracellular solution. The pipette solution contained (in mM): D-gluconic acid potassium salt, 115; KCl, 26; $MgCl_2$, 1; EGTA, 5; HEPES, 10; pH 7.2 with KOH. The specific BK channel inhibitor paxilline (Alomone Labs, Jerusalem, Israel) was used in 5 µM to verify the functional expression of the channels. V_m values were determined following 2 minutes of stable membrane potential recording with I = 0 on Axon 200A/B amplifiers (Lewis et al., 2011). Only cells with seal resistance above 10 GΩ and good access (Rs < 20) were used. Whole-cell currents were recorded in n = 27 CPC and 7 MSC cells. For RMP measurements, all values are quoted as mean ± SEM, with sample size (n) = 22 (CPC) and 8 (MSC). All membrane potentials are corrected for liquid junction potentials estimated using JPCalc (Barry & Lynch, 1991).

9. Measurement of intracellular Ca^{2+} oscillations in CPCs

Cells were loaded with 10 μM Fura-2-AM for 50 mins at 37°C in a CO_2 incubator. After loading, cells were kept in Tyrode's solution and placed on the stage of a ZEISS Axiovert 200m inverted microscope (Zeiss, Oberkochen, Germany) equipped with a Plan-Neofluar 20× objective (NA = 0.5). Fura-2 was excited with a CoolLED pE-340fura light source (CoolLED LTD, Andover, England). Illumination was alternating between 340 and 380 nm wavelength and the emitted fluorescent light was measured through a band-pass filter (505–570 nm) and digitized at 16 bit with an AXIOCam MR3 monochrome camera (Zeiss, Oberkochen, Germany) at a frequency of 12 frames/min. Image acquisition and post processing were carried out with the AxioVision (rel. 4.8) software (Zeiss). The cells were examined in resting conditions for 15 mins at room temperature. At the end of the experiments, 180 μM ATP was added to the bath to check the viability of the cells. Cells not responding to the ATP challenge were excluded from analysis. Intracellular Ca^{2+} concentration ($[Ca^{2+}]_i$) was calculated from the ratio of the images taken at 340 and 380 nm after background correction with constants determined during *in vitro* calibration of the setup. The cells were classified as active if the increase of $[Ca^{2+}]_i$ was more than 10% of the resting level. $n = 332$ cells were analysed.

10. Statistical analysis

All data are representative of at least three independent experiments (biological replicates). RT-qPCR, cell proliferation and mitochondrial activity, as well as cell migration data are expressed as mean ± SEM, DEP data are expressed as mean ± SD. Statistical analysis was performed using Student's unpaired two-tailed *t*-test (*$P < 0.05$; **$P < 0.01$; ***$P < 0.001$).

Results

1. Affymetrix analysis reveals differentially expressed ion channel genes in migratory CPCs

We performed principal component analysis (PCA) of the Affymetrix data on normalized samples to explore their interrelationships (Fig. 1). Biological replicates within the CPC/MSC groups were separated into two distinct clusters, showing that the pattern of gene expression was different in CPCs and MSCs. In total, 3214 genes showed significantly different expression levels between CPC and MSC cells, with 2379 genes being down-regulated and 835 genes up-regulated. Using CytoScape software with the ClueGo application we identified those GO Biological process terms which were over-represented in our gene list. When we analysed the full gene list (up and down-regulated genes together), and the list of down-regulated genes, we found that mainly cell cycle-related categories such as cell cycle, regulation of cell cycle, cell cycle checkpoint, and mitotic/meiotic cell cycle processes were enriched. Furthermore, DNA/nucleic acid metabolism-related pathways were also overrepresented. Separate analyses of up-regulated genes indicated the enrichment of different types of tissue development and cell proliferation processes, such as skin development and mesenchymal cell proliferation (Figure S1 in the Supporting Information (Supplementary File #1); see also Supplementary File #2).

To characterise the expression profiles of genes encoding ion channel subunits in CPCs and to identify differences in expression levels compared to MSCs, we further explored the microarray analysis data. We assessed genes encoding ion channels and transporters commonly involved in regulating potassium, sodium and chloride transport, and calcium homeostasis in chondrocytes (Fig. 2; see also Tables S1-S4 in the Supporting Information). The expression levels for some of the genes studied were different in migratory CPCs *vs*. MSCs. Genes encoding members of the calcium-activated potassium channels (K_{Ca}) showed the most

prominent expression changes; *KCNMA1* and *KCNN4*, the genes coding for the pore forming alpha subunit of the large conductance calcium-activated potassium channel ($K_{Ca}1.1$), and the intermediate/small conductance calcium-activated potassium channel ($K_{Ca}3.1$), respectively. In both cases, there was a more than 1.5-fold upregulation in CPCs. In contrast, the small conductance calcium-activated potassium channel ($K_{Ca}2.3$) encoded by the *KCNN3* gene was unchanged. The β4 regulatory subunit of the large conductance calcium-activated potassium channel (*KCNMB4*) was significantly downregulated in CPCs. *KCNB1* (voltage-gated potassium channel subunit Kv2.1); *KCND2* (Kv4.2) and *KCNH6* (Kv11.2) were also downregulated in CPCs (Table S1 in the Supporting Information).

Whilst most of the genes coding for the alpha subunits of voltage-gated sodium channels were upregulated in CPCs, with *SCN2A* encoding the $Na_V1.2$ sodium channel showing a 1.3-fold upregulation, all epithelial sodium channel (ENaC) subunit genes (*SCNN1A*, *SCNN1B*, *SCNN1D*, *SCNN1G*) were found to show a trend towards downregulation (Table S2 in the Supporting Information), suggesting an altered K^+/Na^+ ion handling in CPCs. The only gene showing a significantly lower expression in CPCs was *SCNN1D*. We also checked the expression patterns of genes encoding the alpha and beta subunits of the Na^+/K^+-ATPase and found that the *ATP1A1* gene was significantly downregulated in CPCs. Genes coding for the rest of the subunits were unchanged.

Interesting differences were found also in the expression patterns of genes coding for proteins involved in global calcium handling. The genes coding for molecules that regulate store-operated calcium entry (SOCE); inositol 1,4,5-trisphosphate receptors (IP_3Rs) that mediate calcium release from the intracellular calcium stores; as well as the sarcoplasmic/endoplasmic reticulum Ca^{2+} ATPase (SERCA) that are responsible for calcium sequestration were showing a trend for downregulation in CPCs. Transcript levels of both *ORAI2* and *ATP2A3* (sarcoplasmic/endoplasmic reticulum calcium ATPase 3) displayed a

significant reduction in CPCs. In contrast, genes coding for voltage-gated calcium channel subunits were unchanged. In a similar way, the ATPases and exchangers that mediate calcium extrusion (*PMCA2-4*, as well as *NCX1-2*); as well as the metabotropic purinergic receptors were also unchanged with a trend towards upregulation, with the exception of *P2RY2*, which was significantly downregulated in CPCs. The genes coding for nonselective cation channels, including members of the ionotropic P2X purinergic receptors, as well as the transient receptor potential cation channel families TRPC and TRPV were showing a general trend towards downregulation, in particular *TRPC4* and *TRPV2* (Table S3 in the Supporting Information).

We have also looked at other ion channel expression patterns and found that the only gene which had a significantly different expression (downregulation in CPCs) between the two cell types was *ASIC1* coding for the acid-sensitive cation channel subunit 1. None of the other transcripts showed significantly different expression levels between CPCs and MSCs (Table S4 in the Supporting Information).

2. Validating microarray data by RT-qPCR confirmed the differential expression of ion channel genes in CPCs

The mRNA expression profiles of selected candidate genes encoding various ion channel subunits were first validated using custom-configured TaqMan 96-Well Fast Gene Expression Array plates (see Tables S5–S6 in the Supporting Information). Given their role in chondroprogenitor and chondrocyte physiology, we were particularly interested in studying the roles of the calcium-activated potassium channels, and therefore we looked at the expression patterns of the genes encoding the various subunits of these channels in details. To confirm the expression patterns of these genes, we employed custom-designed primers and performed individual qPCR reactions. The genes coding for the α and β subunits of the large conductance calcium-activated potassium channel (BK) were all detected; *KCNMA1* and *KCNMB4* were

upregulated; *KCNMB1* was downregulated in CPCs; *KCNMB2* and *KCNMB3* were unchanged. Of the genes encoding the small conductance calcium-activated potassium channel proteins 1–3 (*KCNN1–3*), *KCNN1* was unchanged, whereas *KCNN3* was massively downregulated in CPCs. The gene for the intermediate conductance calcium-activated potassium channel protein 4 (*KCNN4*) was showing a significant downregulation in CPCs (Fig. 3). Differences were detected between our qRT-PCR and microarray data. This has been observed before and is largely attributed to the differences in probe sequences (Canales et al., 2006); however, the observed differences could also be attributable to different methodological aspects of the two approaches, such as the fundamentally different data normalization strategies (Morey et al., 2006).

3. Modulation of the BK potassium channel alters cell proliferation, marker gene expression and migration of CPCs

To assess the role of large conductance calcium-activated potassium channels in CPCs and MSCs on cell proliferation and viability (mitochondrial activity), cells were incubated in the presence of the selective BK channel inhibitors iberiotoxin (IBTX; 100 nM) and paxilline (1 μM); or the BK channel activator NS1619 (10 μM) prior to assays. Whilst none of the tested compounds interfered with the mitochondrial activity of the cells (i.e. did not have adverse effects on general cell physiology; Fig. 4A), both IBTX and paxilline significantly reduced the proliferation rate in CPCs, but had no significant effect in MSCs (Fig. 4B; see also Figure S2 in the Supporting Information). When CPCs were cultured in the presence of 1 μM paxilline, the osteogenic transcription factor *RUNX2* was significantly upregulated compared to the control, whereas the expression profile of *SOX9*, the chondrogenic master regulator, remained unchanged. *COL1A1*, on the other hand, was upregulated following paxilline treatment (Fig. 4C).

Given that the CPCs employed in this study have previously been demonstrated *in vitro* and *in vivo* migratory features (Koelling et al., 2009), we performed two different migration assays with or without the BK channel inhibitor paxilline. Fibronectin-guided migration of CPCs in a Boyden chemotaxis chamber was significantly increased in the presence of 1 μM paxilline (Fig. 5A). The effect of paxilline was also examined in random cell migration assays. Paxilline at 1 μM enhanced the migratory parameters of chondroprogenitor cells, significantly increased the total path of migration, the maximum distance from the origin; furthermore, the average cell speed was also significantly greater compared to the control (Fig. 5B). Next, we shifted the migratory tracks (total paths) of the individual cells to a common origin to generate static wind rose plots (Fig. 5C). The bigger diameter of the wind rose plot in paxilline-treated cells indicates the increased motility of these cells.

4. Electrophysiological properties and intracellular calcium oscillations of chondroprogenitor cells

CPC and MSC cell lines with a characteristic mesenchymal morphology were grown under standard culturing conditions prior to preparation for DEP analysis (Fig. 6A). The measured DEP spectra of the cell lines were used to determine specific membrane capacitance (C_{spec}) and conductance (G_{spec}) values; as these calculations take cell size into account (the values of capacitance and conductance are cell size independent), the cell radii were determined after trypsinisation, which were statistically different. The electrophysiological properties of CPC and MSC cells are shown in Fig. 6B, and summarised in Table 1. Effective membrane capacitance (C_{Eff}) is a measure of the ability of the membrane to store charge and generate a dipole in a frequency-dependent manner in DEP. The C_{Eff} values of CPC and MSC cells were not significantly different from each other. The membrane capacitance per cell area values were also very similar between CPC and MSC. The intracellular conductivities of CPC and MSC

were also almost identical between the two cell types. The greatest difference between the two cell types was seen with regards to the specific membrane conductance (G_{Spec}) parameter: CPCs were characterised by a significantly higher G_{Spec} value than MSCs, which equals to a 32.8% difference. Representative DEP spectra for CPC and MSC cells are shown in Fig. 6C.

As RT-qPCR analysis revealed changes in the expression of several ion channels at the mRNA level, whole cell currents were examined. Both CPC and MSC cells were heterogeneous in respect to ionic current expression. Significant current was recorded in 6 out of 27 CPC cells. The voltage dependent features of these outward currents were reminiscent of that of BK channels. In addition, the time-dependent component was inhibited by paxilline, indicating that the current was partially carried by BK channels. The linear component of the current was not specified further. In a similar way, paxilline-sensitive composite current was observed in 4 out of 7 MSC cells (Fig. 7A–B). The resting membrane potential of CPCs did not differ significantly from that of MSCs as determined by whole-cell patch clamp measurements (–24.1 mV *vs*. –21.3 mV) (Fig. 7C).

Since CPCs have been previously described to display oscillations in cytosolic calcium levels, we also looked at whether paxilline interfered with these spontaneous calcium events. In control cultures, 16% of CPCs exhibited periodic changes in cytosolic Ca^{2+} concentration (n = 112), but 1 μM paxilline completely abolished such events (n = 83) (Fig. 7D).

Discussion

OA is a multi-faceted and highly heterogenous whole-joint disease without a common pathophysiological pathway. Therefore, it is unlikely that a single therapeutic target can change the course of disease progression. There are currently no therapeutic strategies able to halt or significantly delay OA progression, and the existing pharmacological treatments are unable to sustain effective and long-lasting symptomatic relief. At present, joint replacement with an

artificial prosthesis is the single most effective measure to improve patient quality of life, but of course not all OA patients will progress to this stage (Conaghan et al., 2019). To develop novel therapeutic approaches targeting OA, a more profound understanding of the molecular mechanisms of the disease is required. A broad spectrum of ongoing trials and treatment options target various aspects of the disease, including cartilage and bone regeneration or repair, inflammatory and pain processes, altered metabolic pathways, and senescence (Grassel & Muschter, 2020).

Certain stem cell-based cartilage regenerative approaches are already in phase I clinical study stage. BM-MSCs and adipose tissue-derived MSCs (AD-MSCs) are currently the preferred cell types for regenerative strategies (Grassel & Muschter, 2020). However, whether MSCs are really the optimal cell population for cartilage regenerative therapy is still controversial. In this study, we turned our attention to alternative cell sources with potentially superior chondrogenic potential compared to BM-MSCs, which could be exploited for future cartilage regenerative therapies. Migratory CPCs have been partially characterised; they are known to exhibit a distinct transcriptomic signature compared to osteoblasts, chondrocytes and immortalised foetal chondrocytes (T/C-28 cells) (Koelling et al., 2009). However, the specific cellular identity and detailed molecular phenotype of CPCs is still elusive. Therefore, the aim of this study was to elucidate the biology and phenotype of CPCs by comparing their transcriptomic profile with BM-MSCs. Given the unique ionic composition of the CPC niche within the ECM of diseased cartilage, we were especially interested in differences in the channelome of CPCs, focusing on K^+ and Ca^{2+} transporters potentially involved in maintaining the progenitor phenotype under inflammatory conditions. We also mapped the electrophysiological profile of CPCs using patch-clamp and DEP.

We have recently analysed the surfaceome of CPCs using selective cell surface protein labelling followed by high-throughput mass spectrometry and identified alterations in the

composition of the surfaceome compared to BM-MSCs (Matta et al., 2019). However, even the high-throughput mass spectrometry-based approach that we employed was not sensitive enough to detect alterations in very low-abundance ion channels and transporters. Here, we performed microarray analysis and compared the global gene expression signatures of CPCs to BM-MSCs. CPCs harboured a distinct transcriptomic profile and mRNA expression pattern that was different to that of MSCs. Pathway analysis confirmed that mainly cell cycle-related and DNA/nucleic acid metabolism related GO categories were overrepresented in the list of genes with significantly different expression levels, which was clearly reflected by the lower proliferation rate of CPCs compared to MSCs. There was a 64% correlation with the direction of fold changes of differentially expressed transporter genes when we compared their pattern to the data generated by quantitative mass spectrometric analysis on the surfaceome of CPC and MSC cells (Table S8 in the Supporting information; see also Supplementary file #2) (Matta et al., 2019).

Differential K^+ transporter gene expression profiles in CPCs

We chose to study the expression profiles of those ion channel and transporter families that may have a relevance in chondroprogenitor cell physiology (Barrett-Jolley et al., 2010; Matta & Zakany, 2013; Mobasheri et al., 2019). The most widely reported ion channels in chondrocytes and MSCs are potassium channels (Mobasheri et al., 2012; Pchelintseva & Djamgoz, 2018). The human genome contains around 70 different potassium channel genes, which makes them the largest family of membrane ion channels (Mobasheri et al., 2012). The α-subunit (*KCNMA1*) of the large conductance Ca^{2+}-activated potassium channel (BK, BK_{Ca}, MaxiK), as well as the intermediate Ca^{2+}-activated potassium channel (IK, KCNN4, SK4, $K_{Ca}3.1$) transcripts displayed the largest fold changes, with a 50% upregulation in CPCs. BK channels have been detected in undifferentiated MSCs both at the mRNA level and by single

channel recordings (Kawano et al., 2003), and also in mature chondrocytes (Mobasheri et al., 2010). BK channels may play various roles in chondrocyte physiology including volume regulation, oxygen sensing, and mechanotransduction (Mobasheri et al., 2012). Since BK channels have been implicated in driving MSC differentiation (Pchelintseva & Djamgoz, 2018), perhaps the fact that CPCs are more committed to the chondrogenic lineage than undifferentiated MSCs may explain the higher levels of *KCNMA1* both at the transcript and at the protein level (Matta et al., 2019).

BK channels may also be potential drug targets to protect against joint degeneration in OA (Haidar et al., 2020). In an *in vitro* model of synovial inflammation, *KCNMA1* was found to be upregulated following cytokine treatment in primary synovial fibroblasts (Haidar et al., 2020). BK channel expression was also found to be upregulated in human OA cartilage (Lewis et al., 2013). Given that the migratory CPCs used in this study had been isolated from late-stage OA, the increased *KCNMA1* expression may also be a result of their original inflammatory niche.

To further characterise the contribution of BK channels to the chondroprogenitor phenotype, we first looked at whether BK channel function was required for cell division. The role of BK channels in mediating proliferation has been controversial. BK channels are known to stimulate proliferation in BM-MSCs (Zhang et al., 2014); however, their activation may also lead to anti-proliferative effects in human induced pluripotent stem cell (hiPSC)-derived MSCs (Zhao et al., 2013). The BK channel inhibitors paxilline and IBTX have significantly lowered the proliferation rate of CPCs, but not in MSCs. This may be attributed to the different sensitivity of the two cell types to BK channel inhibition, and the dose-dependent effect of paxilline on proliferation. Whilst 1 μM paxilline caused a ~10% reduction in DNA synthesis in BM-MSCs, at 3 μM it resulted in ~80% inhibition (Zhang et al., 2014). On the other hand,

in line with our data, IBTX did not alter [^{3}H]-thymidine incorporation levels in rat BM-MSCs (Deng et al., 2007).

The increased abundance of *KCNN4* transcripts in CPCs may reflect their inherently enhanced cell motility as IK channels have a confirmed role in migration (Pchelintseva & Djamgoz, 2018). In contrast, BK channels have a rather controversial role in cell motility (Catacuzzeno et al., 2015). In migratory CPCs, BK channels may play an inhibitory role in the motility of the cells as paxilline treatment increased every parameters of migration. These findings are rather unexpected as the BK channel inhibitor iberiotoxin was reported to block the platelet lysate-induced migration of MSCs (Echeverry et al., 2020). In glioma cells, however, BK channel openers inhibited migration (Kraft et al., 2003). Given that CPCs express both *SOX9* and *RUNX2* and that there is a degree of crosstalk between these transcription factors (Koelling et al., 2009), perhaps BK blockade influenced CPC behaviour in such a way that it attenuated their chondrogenic phenotype, which is also reflected in the upregulation of the osteogenic transcription factor *RUNX2*.

$Ca2^+$ homeostasis in chondroprogenitor cells

Given that BK channel function depends on both RMP and $[Ca^{2+}]_i$, we undertook to look at the transporters mediating the Ca^{2+} homeostasis of the chondroprogenitor cells. Calcium plays central roles in cell physiology in non-excitable cells such as chondrocytes (Suzuki et al., 2020). Dynamic changes in calcium signalling has been shown to be paramount to chondrogenesis (Matta & Zakany, 2013), and we have described earlier the calcium handling in CPCs (Matta et al., 2015). Store-operated Ca^{2+} entry (SOCE), one of the main sources of Ca^{2+} influx, is mediated by Ca^{2+} release-activated Ca^{2+} channels (CRAC) formed of ORAI1, ORAI2 and ORAI3 proteins. We found that *ORAI2* was present in lower abundance in CPCs; ORAI2 has been reported to modulate the magnitude of SOCE (Inayama et al., 2015; Vaeth et

al., 2017), which further pinpoints the important role of SOCE in CPC homeostasis. Given that purinergic signalling regulates intracellular Ca^{2+} oscillations in CPCs and MSCs (Jiang et al., 2017; Matta et al., 2015), we also looked at differences in purinergic receptor transcript levels. The only gene with a significantly altered expression was *P2RY2*, which codes for a metabotropic receptor involved in the negative regulation of the osteogenic differentiation of BM-MSCs (Li et al., 2016).

BK channel function was reported to modulate $[Ca^{2+}]_i$ oscillations in various cell types (Mizutani et al., 2016; Wakle-Prabagaran et al., 2016). Both CPCs (Matta et al., 2015) and MSCs (Kawano et al., 2003) are known to exhibit periodic fluctuations in resting cytosolic Ca^{2+} levels. We confirmed that BK channels play a central role in mediating the Ca^{2+} homeostasis in CPCs, since the BK channel inhibitor paxilline completely abolished these $[Ca^{2+}]_i$ oscillations. This is the first study to report a mechanistic link between the big conductance calcium-sensitive potassium channels and periodic $[Ca^{2+}]_i$ oscillations in chondroprogenitor cells.

Electrophysiological profiling of CPCs

Having established the channelome of CPCs at the transcript level, we then looked at whether the global electrophysiological profile (electrome) of the progenitor cells was different from that of BM-MSCs. In addition to conventional patch clamping, we also employed DEP, which has been shown to be an efficient quantitative method of differentiating between closely related cell types e.g. in the bone marrow (Ismail et al., 2015). DEP can be used for both assessing the passive electrical properties of cellular components, and as the basis for a separation method (Mahabadi et al., 2018). This could be especially relevant for CPCs present at very low abundance in arthritic cartilage, given that a truly reliable cell surface marker has still not been identified. Inherent cell properties that do not require the use of specific labelling

for detection would provide a unique means to identify progenitors committed to particular cell fates. Whilst the effective membrane capacitance and the intracellular conductivity values did not differ, we report membrane conductance as a specific electrophysiological property that reflects the differentiation stage of human CPCs and MSCs. Membrane conductivity is a parameter that describes the potential of the membrane to transmit charge; and is indicative of ionic flux (Henslee et al., 2017).

We employed patch clamping to establish the RMP of CPCs, which was not statistically different from that of MSCs. The V_m value of MSCs detected in our study (approx. –20 mV) was similar to what has been observed earlier (–10 mV) (Kawano et al., 2003). The RMP of mature chondrocytes is dependent on the coordinated function of different types of ion channels including non-selective cation channels (Lewis et al., 2011) and K^+ channels (Maleckar et al., 2018; Wilson et al., 2004). The majority of these channels did not show statistically different expression between MSCs and CPCs, which probably explains why there is no difference in RMP as observed in this study. As described above, various K^+ channels were detected at the transcript level in both cell types; therefore, we studied the outward whole cell currents in CPC and MSC cells. Both cell populations were heterogeneous with respect to ion current expression, and we found evidence of paxilline-sensitive conductances.

Summary and Conclusions

Here we have provided evidence, for the first time, that BK channels were functional in undifferentiated CPCs, as the voltage dependent features of the detected potassium currents were reminiscent of that of BK channels. In addition, the time-dependent component was inhibited by paxilline, indicating that the current was partially carried by BK channels. Functional BK channels were required for maintaining the balanced differentiation state of

CPCs as paxilline treatment significantly upregulated the osteogenic transcription factor *RUNX2*, which favours osteogenic differentiation potentials.

In line with our previous paper describing the Ca^{2+} homeostasis of CPCs (Matta et al., 2015), here we provide experimental data supporting the hypothesis that periodic increases in $[Ca^{2+}]_i$ may activate BK channels. The ionic fluxes mediated by these channels may alter the RMP, which in turn modulates Ca^{2+} influx. Such a feedback loop has been recently proposed to exist in chondrocytes (Suzuki et al., 2020); we have now identified the key components of that loop in CPCs in this work. It is plausible to hypothesise that under resting conditions, the $[Ca^{2+}]_i$ peaks could activate BK channels to such an extent that the K^+ efflux they mediate does not favour the changes in cell volume and shape required for cell migration.

Perspectives

A recent systematic review has analysed the outcome of 17 studies assessing articular cartilage repair after the clinical application of cell populations containing MSCs in human subjects with knee osteoarthritis (Ha et al., 2019). Significantly better clinical outcomes (improvement of the cartilage state on magnetic resonance imaging or repaired tissue on second-look arthroscopy) were reported in the MSC group in most of the studies. However, there is limited evidence to support the efficacy of intra-articular MSC-based therapy. This highlights opportunities for identifying alternative cell sources. Whilst the preferred cells used were bone, adipose tissue or umbilical cord-derived mesenchymal stem cells, perhaps exploiting the resident cartilage progenitor cell population present in both healthy and OA cartilage may further enhance the efficacy of such novel therapies. We demonstrate here that CPCs are a distinct cell population but are still similar to BM-MSCs in many ways. This work adds key mechanistic and cellular phenotype data to the in-depth characterisation of cartilage

progenitor cells; however, further research is necessary to reconstruct the progenitor niche which would promote their hyaline cartilage regenerative potential.

Supplementary Materials

The following supplementary materials are published online alongside the manuscript.

Supplementary File 1 (PDF): Tables S1–S8; Figures S1–S2.

Supplementary File 2 (PNG): Graphical output of over-represented Gene ontology (GO) pathways in CPCs *vs* MSCs after analysing the full list of differentially expressed genes with Cytospace CluGO. Circles represent the distinct terms, and arrows show the relationship between them. Terms related to cell cycle and DNA metabolism were enriched.

Supplementary File 3 (XLSX): Correlation analysis between surfaceome proteins and their genes.

Acknowledgements

The authors are thankful to Mrs Krisztina Bíróné Barna for skilful technical assistance. We would also like to acknowledge the contribution of Drs William Kothalawala Jayasekara and Roland Ádám Takács.

Funding

C.M. was supported by the European Commission through a Marie Skłodowska-Curie Intra-European Fellowship for career development (project number: 625746; acronym: CHONDRION; FP7-PEOPLE-2013-IEF), the Premium Postdoctoral Research Fellowship of the Eötvös Loránd Research Network (ELKH), and the Young Researcher Excellence Programme (grant number: FK 134304) of the National Research, Development and

Innovation Office, Hungary. Project no. TKP2020-NKA-04 has been implemented with the support provided from the National Research, Development and Innovation Fund of Hungary, financed under the 2020-4.1.1-TKP2020 funding scheme. AM was the co-ordinator of the D-BOARD Consortium funded by European Commission Framework 7 programme (EU FP7; HEALTH.2012.2.4.5-2, project number 305815, Novel Diagnostics and Biomarkers for Early Identification of Chronic Inflammatory Joint Diseases). A.M. has received funding from the Deanship of Scientific Research (DSR), King AbdulAziz University (grant no. 1-141/1434 HiCi). AM is a member of the Arthritis Research UK Centre for Sport, Exercise, and Osteoarthritis, funded by Arthritis Research UK (Grant Reference Number: 20194). AM wishes to acknowledge financial support from the European Structural and Social Funds (ES Struktūrinės Paramos) through the Research Council of Lithuania (Lietuvos Mokslo Taryba) according to the activity 'Improvement of researchers' qualification by implementing world-class R&D projects' of Measure No. 09.3.3-LMT-K-712 (grant application code: 09.3.3-LMT-K-712-01-0157, agreement No. DOTSUT-215) and the new funding programme: Attracting Foreign Researchers for Research Implementation (2018-2022), Grant No 01.2.2-LMT-K-718-02-0022. A.K-P. was supported by the National Research, Development and Innovation Office of Hungary (grant number: FK 134684), and by the GINOP-2.3.2-15-2016-00040 project.

Availability of Data and Material

The data set is published in a MIAME compliant format in the GEO database (http://www.ncbi.nlm.nih.gov/geo/); accession numbers: GSM4885525-GSM4485530 (GSE160886). **Reviewer token: chanoygyjbudnun**. All other data generated or analysed during this study are included in this published article [and its supplementary information files].

Author Contributions

Conceptualization, C.M. and A.M.; Methodology, C.M., R.L., C.F., J.A., S.M., P.S., A.K-P., M.P.H., A.M.; Software, M.C.U., S.P., J.F., A.K-P., F.L., M.P.H.; Validation, C.M., C.F., S.P.; Formal Analysis, C.M., R.L., C.F., E.H., J.F., J.A., F.L.; Investigation, C.M., R.L., C.F., G.D., M.C.U., S.P., P.S, T.H., E.H.; Resources, J.A., S.M., J.D., N.M., R.B.J., P.S., A.K-P., M.P.H., A.M.; Data Curation, C.M., R.L., C.F., J.A., J.F., T.H., M.C.U., E.H.; Writing – Original Draft Preparation, C.M., R.L.; Writing – Review & Editing, all authors; Visualization, C.M., M.C.U., G.D., S.P., J.F., A.K-P., E.H.; Supervision, N.M., R.B.J., F.L., J.D., S.M., P.S., A.K-P., A.M.; Project Administration, C.M., A.M.; Funding Acquisition, C.M., A.M.

Conflicts of Interest

The authors declare that they have no competing interests. This paper was written by the authors within the scope of their academic and research positions. None of the authors have any relationships that could be construed as biased or inappropriate. The funding bodies were not involved in the study design, data collection, analysis and interpretation. The decision to submit the paper for publication was not influenced by any the funding bodies.

References

Al Maini, M., Al Weshahi, Y., Foster, H. E., Chehade, M. J., Gabriel, S. E., Saleh, J. A., Al Wahshi, H., Bijlsma, J. W. J., Cutolo, M., Lakhanpal, S., Venkatramana, M., Pineda, C., & Woolf, A. D. (2020). A global perspective on the challenges and opportunities in learning about rheumatic and musculoskeletal diseases in undergraduate medical education : White paper by the World Forum on Rheumatic and Musculoskeletal Diseases (WFRMD). *Clin Rheumatol*, *39*(3), 627-642. https://doi.org/10.1007/s10067-019-04544-y

Almassy, J., & Begenisich, T. (2012). The LRRC26 protein selectively alters the efficacy of BK channel activators. *Mol Pharmacol*, *81*(1), 21-30. https://doi.org/10.1124/mol.111.075234

Andersen, C. L., Jensen, J. L., & Orntoft, T. F. (2004). Normalization of real-time quantitative reverse transcription-PCR data: a model-based variance estimation approach to identify genes suited for normalization, applied to bladder and colon cancer data sets. *Cancer Res*, *64*(15), 5245-5250. https://doi.org/10.1158/0008-5472.CAN-04-0496

Archer, C. W., & Francis-West, P. (2003). The chondrocyte. *Int J Biochem Cell Biol*, *35*(4), 401-404. https://doi.org/10.1016/s1357-2725(02)00301-1

Asmar, A., Barrett-Jolley, R., Werner, A., Kelly, R., Jr., & Stacey, M. (2016). Membrane channel gene expression in human costal and articular chondrocytes. *Organogenesis*, *12*(2), 94-107. https://doi.org/10.1080/15476278.2016.1181238

Barrett-Jolley, R., Lewis, R., Fallman, R., & Mobasheri, A. (2010). The emerging chondrocyte channelome. *Front Physiol*, *1*, 135. https://doi.org/10.3389/fphys.2010.00135

Barry, P. H., & Lynch, J. W. (1991). Liquid junction potentials and small cell effects in patch-clamp analysis. *J Membr Biol*, *121*(2), 101-117. https://doi.org/10.1007/BF01870526

Broche, L. M., Labeed, F. H., & Hughes, M. P. (2005). Extraction of dielectric properties of multiple populations from dielectrophoretic collection spectrum data. *Phys Med Biol*, *50*(10), 2267-2274. https://doi.org/10.1088/0031-9155/50/10/006

Buckwalter, J. A., Mankin, H. J., & Grodzinsky, A. J. (2005). Articular cartilage and osteoarthritis. *Instr Course Lect*, *54*, 465-480. https://www.ncbi.nlm.nih.gov/pubmed/15952258

Canales, R. D., Luo, Y., Willey, J. C., Austermiller, B., Barbacioru, C. C., Boysen, C., Hunkapiller, K., Jensen, R. V., Knight, C. R., Lee, K. Y., Ma, Y., Maqsodi, B., Papallo, A., Peters, E. H., Poulter, K., Ruppel, P. L., Samaha, R. R., Shi, L., Yang, W., Zhang, L., & Goodsaid, F. M. (2006). Evaluation of DNA microarray results with quantitative gene expression platforms. *Nat Biotechnol*, *24*(9), 1115-1122. https://doi.org/10.1038/nbt1236

Catacuzzeno, L., Caramia, M., Sforna, L., Belia, S., Guglielmi, L., D'Adamo, M. C., Pessia, M., & Franciolini, F. (2015). Reconciling the discrepancies on the involvement of large-conductance Ca(2+)-activated K channels in glioblastoma cell migration. *Front Cell Neurosci*, *9*, 152. https://doi.org/10.3389/fncel.2015.00152

Conaghan, P. G., Cook, A. D., Hamilton, J. A., & Tak, P. P. (2019). Therapeutic options for targeting inflammatory osteoarthritis pain. *Nat Rev Rheumatol*, *15*(6), 355-363. https://doi.org/10.1038/s41584-019-0221-y

De Loof, A. (2016). The cell's self-generated "electrome": The biophysical essence of the immaterial dimension of Life? *Commun Integr Biol*, *9*(5), e1197446. https://doi.org/10.1080/19420889.2016.1197446

Deng, X. L., Lau, C. P., Lai, K., Cheung, K. F., Lau, G. K., & Li, G. R. (2007). Cell cycle-dependent expression of potassium channels and cell proliferation in rat mesenchymal stem cells from bone marrow. *Cell Prolif*, *40*(5), 656-670. https://doi.org/10.1111/j.1365-2184.2007.00458.x

Dowthwaite, G. P., Bishop, J. C., Redman, S. N., Khan, I. M., Rooney, P., Evans, D. J., Haughton, L., Bayram, Z., Boyer, S., Thomson, B., Wolfe, M. S., & Archer, C. W. (2004). The surface of articular cartilage contains a progenitor cell population. *J Cell Sci*, *117*(Pt 6), 889-897. https://doi.org/10.1242/jcs.00912

Echeverry, S., Grismaldo, A., Sanchez, C., Sierra, C., Henao, J. C., Granados, S. T., Sutachan, J. J., & Torres, Y. P. (2020). Activation of BK Channel Contributes to PL-Induced Mesenchymal Stem Cell Migration. *Front Physiol*, *11*, 210. https://doi.org/10.3389/fphys.2020.00210

Fellows, C. R., Williams, R., Davies, I. R., Gohil, K., Baird, D. M., Fairclough, J., Rooney, P., Archer, C. W., & Khan, I. M. (2017). Characterisation of a divergent progenitor cell sub-populations in human osteoarthritic cartilage: the role of telomere erosion and replicative senescence. *Sci Rep*, *7*, 41421. https://doi.org/10.1038/srep41421

Gomoll, A. H., & Minas, T. (2014). The quality of healing: articular cartilage. *Wound Repair Regen*, *22 Suppl 1*, 30-38. https://doi.org/10.1111/wrr.12166

Grassel, S., & Muschter, D. (2020). Recent advances in the treatment of osteoarthritis. *F1000Res*, *9*. https://doi.org/10.12688/f1000research.22115.1

Ha, C. W., Park, Y. B., Kim, S. H., & Lee, H. J. (2019). Intra-articular Mesenchymal Stem Cells in Osteoarthritis of the Knee: A Systematic Review of Clinical Outcomes and Evidence of Cartilage Repair. *Arthroscopy*, *35*(1), 277-288 e272. https://doi.org/10.1016/j.arthro.2018.07.028

Haidar, O., O'Neill, N., Staunton, C. A., Bavan, S., O'Brien, F., Zouggari, S., Sharif, U., Mobasheri, A., Kumagai, K., & Barrett-Jolley, R. (2020). Pro-inflammatory Cytokines Drive Deregulation of Potassium Channel Expression in Primary Synovial Fibroblasts. *Front Physiol*, *11*, 226. https://doi.org/10.3389/fphys.2020.00226

Hdud, I. M., Mobasheri, A., & Loughna, P. T. (2014). Effect of osmotic stress on the expression of TRPV4 and BKCa channels and possible interaction with ERK1/2 and p38 in cultured equine chondrocytes. *Am J Physiol Cell Physiol*, *306*(11), C1050-1057. https://doi.org/10.1152/ajpcell.00287.2013

Henrotin, Y., Sanchez, C., Bay-Jensen, A. C., & Mobasheri, A. (2016). Osteoarthritis biomarkers derived from cartilage extracellular matrix: Current status and future perspectives. *Ann Phys Rehabil Med*, *59*(3), 145-148. https://doi.org/10.1016/j.rehab.2016.03.004

Henslee, E. A., Crosby, P., Kitcatt, S. J., Parry, J. S. W., Bernardini, A., Abdallat, R. G., Braun, G., Fatoyinbo, H. O., Harrison, E. J., Edgar, R. S., Hoettges, K. F., Reddy, A. B., Jabr, R. I., von Schantz, M., O'Neill, J. S., & Labeed, F. H. (2017). Rhythmic potassium transport regulates the circadian clock in human red blood cells. *Nat Commun*, *8*(1), 1978. https://doi.org/10.1038/s41467-017-02161-4

Hoettges, K. F., Henslee, E. A., Torcal Serrano, R. M., Jabr, R. I., Abdallat, R. G., Beale, A. D., Waheed, A., Camelliti, P., Fry, C. H., van der Veen, D. R., Labeed, F. H., & Hughes, M. P. (2019). Ten-Second Electrophysiology: Evaluation of the 3DEP Platform for high-speed, high-accuracy cell analysis. *Sci Rep*, *9*(1), 19153. https://doi.org/10.1038/s41598-019-55579-9

Hoettges, K. F., Hubner, Y., Broche, L. M., Ogin, S. L., Kass, G. E., & Hughes, M. P. (2008). Dielectrophoresis-activated multiwell plate for label-free high-throughput drug assessment. *Anal Chem*, *80*(6), 2063-2068. https://doi.org/10.1021/ac702083g

Hunter, D. J., & Bierma-Zeinstra, S. (2019). Osteoarthritis. *Lancet*, *393*(10182), 1745-1759. https://doi.org/10.1016/S0140-6736(19)30417-9

Inayama, M., Suzuki, Y., Yamada, S., Kurita, T., Yamamura, H., Ohya, S., Giles, W. R., & Imaizumi, Y. (2015). Orai1-Orai2 complex is involved in store-operated calcium entry in chondrocyte cell lines. *Cell Calcium*, *57*(5-6), 337-347. https://doi.org/10.1016/j.ceca.2015.02.005

Ismail, A., Hughes, M. P., Mulhall, H. J., Oreffo, R. O., & Labeed, F. H. (2015). Characterization of human skeletal stem and bone cell populations using dielectrophoresis. *J Tissue Eng Regen Med*, *9*(2), 162-168. https://doi.org/10.1002/term.1629

Jiang, L. H., Mousawi, F., Yang, X., & Roger, S. (2017). ATP-induced Ca(2+)-signalling mechanisms in the regulation of mesenchymal stem cell migration. *Cell Mol Life Sci*, *74*(20), 3697-3710. https://doi.org/10.1007/s00018-017-2545-6

Kawano, S., Otsu, K., Shoji, S., Yamagata, K., & Hiraoka, M. (2003). Ca(2+) oscillations regulated by Na(+)-Ca(2+) exchanger and plasma membrane Ca(2+) pump induce fluctuations of membrane currents and potentials in human mesenchymal stem cells. *Cell Calcium*, *34*(2), 145-156. https://doi.org/10.1016/s0143-4160(03)00069-1

Koelling, S., Kruegel, J., Irmer, M., Path, J. R., Sadowski, B., Miro, X., & Miosge, N. (2009). Migratory chondrogenic progenitor cells from repair tissue during the later stages of

human osteoarthritis. *Cell Stem Cell*, *4*(4), 324-335. https://doi.org/10.1016/j.stem.2009.01.015

Kraft, R., Krause, P., Jung, S., Basrai, D., Liebmann, L., Bolz, J., & Patt, S. (2003). BK channel openers inhibit migration of human glioma cells. *Pflugers Arch*, *446*(2), 248-255. https://doi.org/10.1007/s00424-003-1012-4

Labeed, F. H., Lu, J., Mulhall, H. J., Marchenko, S. A., Hoettges, K. F., Estrada, L. C., Lee, A. P., Hughes, M. P., & Flanagan, L. A. (2011). Biophysical characteristics reveal neural stem cell differentiation potential. *PLoS One*, *6*(9), e25458. https://doi.org/10.1371/journal.pone.0025458

Lewis, R., Asplin, K. E., Bruce, G., Dart, C., Mobasheri, A., & Barrett-Jolley, R. (2011). The role of the membrane potential in chondrocyte volume regulation. *J Cell Physiol*, *226*(11), 2979-2986. https://doi.org/10.1002/jcp.22646

Lewis, R., & Barrett-Jolley, R. (2015). Changes in Membrane Receptors and Ion Channels as Potential Biomarkers for Osteoarthritis. *Front Physiol*, *6*, 357. https://doi.org/10.3389/fphys.2015.00357

Lewis, R., Feetham, C. H., Gentles, L., Penny, J., Tregilgas, L., Tohami, W., Mobasheri, A., & Barrett-Jolley, R. (2013). Benzamil sensitive ion channels contribute to volume regulation in canine chondrocytes. *Br J Pharmacol*, *168*(7), 1584-1596. https://doi.org/10.1111/j.1476-5381.2012.02185.x

Li, W., Wei, S., Liu, C., Song, M., Wu, H., & Yang, Y. (2016). Regulation of the osteogenic and adipogenic differentiation of bone marrow-derived stromal cells by extracellular uridine triphosphate: The role of P2Y2 receptor and ERK1/2 signaling. *Int J Mol Med*, *37*(1), 63-73. https://doi.org/10.3892/ijmm.2015.2400

Loeser, R. F., Goldring, S. R., Scanzello, C. R., & Goldring, M. B. (2012). Osteoarthritis: a disease of the joint as an organ. *Arthritis Rheum*, *64*(6), 1697-1707. https://doi.org/10.1002/art.34453

Mahabadi, S., Labeed, F. H., & Hughes, M. P. (2018). Dielectrophoretic analysis of treated cancer cells for rapid assessment of treatment efficacy. *Electrophoresis*, *39*(8), 1104-1110. https://doi.org/10.1002/elps.201700488

Maleckar, M. M., Clark, R. B., Votta, B., & Giles, W. R. (2018). The Resting Potential and K(+) Currents in Primary Human Articular Chondrocytes. *Front Physiol*, *9*, 974. https://doi.org/10.3389/fphys.2018.00974

Maleckar, M. M., Martin-Vasallo, P., Giles, W. R., & Mobasheri, A. (2020). Physiological Effects of the Electrogenic Current Generated by the Na+/K+ Pump in Mammalian Articular Chondrocytes. *Bioelectricity*, 258-268. https://doi.org/10.1089/bioe.2020.0036

Mankin, H. J., & Lippiello, L. (1970). Biochemical and metabolic abnormalities in articular cartilage from osteo-arthritic human hips. *J Bone Joint Surg Am*, *52*(3), 424-434. https://www.ncbi.nlm.nih.gov/pubmed/4246573

Matta, C., Boocock, D. J., Fellows, C. R., Miosge, N., Dixon, J. E., Liddell, S., Smith, J., & Mobasheri, A. (2019). Molecular phenotyping of the surfaceome of migratory chondroprogenitors and mesenchymal stem cells using biotinylation, glycocapture and quantitative LC-MS/MS proteomic analysis. *Sci Rep*, *9*(1), 9018. https://doi.org/10.1038/s41598-019-44957-y

Matta, C., Fodor, J., Miosge, N., Takacs, R., Juhasz, T., Rybaltovszki, H., Toth, A., Csernoch, L., & Zakany, R. (2015). Purinergic signalling is required for calcium oscillations in migratory chondrogenic progenitor cells. *Pflugers Arch*, *467*(2), 429-442. https://doi.org/10.1007/s00424-014-1529-8

Matta, C., & Zakany, R. (2013). Calcium signalling in chondrogenesis: implications for cartilage repair. *Front Biosci (Schol Ed)*, *5*, 305-324. https://www.ncbi.nlm.nih.gov/pubmed/23277053

Mizutani, H., Yamamura, H., Muramatsu, M., Hagihara, Y., Suzuki, Y., & Imaizumi, Y. (2016). Modulation of Ca2+ oscillation and melatonin secretion by BKCa channel activity in rat pinealocytes. *Am J Physiol Cell Physiol*, *310*(9), C740-747. https://doi.org/10.1152/ajpcell.00342.2015

Mobasheri, A., Lewis, R., Ferreira-Mendes, A., Rufino, A., Dart, C., & Barrett-Jolley, R. (2012). Potassium channels in articular chondrocytes. *Channels (Austin)*, *6*(6), 416-425. https://doi.org/10.4161/chan.22340

Mobasheri, A., Lewis, R., Maxwell, J. E., Hill, C., Womack, M., & Barrett-Jolley, R. (2010). Characterization of a stretch-activated potassium channel in chondrocytes. *J Cell Physiol*, *223*(2), 511-518. https://doi.org/10.1002/jcp.22075

Mobasheri, A., Matta, C., Uzieliene, I., Budd, E., Martin-Vasallo, P., & Bernotiene, E. (2019). The chondrocyte channelome: A narrative review. *Joint Bone Spine*, *86*(1), 29-35. https://doi.org/10.1016/j.jbspin.2018.01.012

Mobasheri, A., Mobasheri, R., Francis, M. J., Trujillo, E., Alvarez de la Rosa, D., & Martin-Vasallo, P. (1998). Ion transport in chondrocytes: membrane transporters involved in intracellular ion homeostasis and the regulation of cell volume, free [Ca2+] and pH. *Histol Histopathol*, *13*(3), 893-910. https://doi.org/10.14670/HH-13.893

Morey, J. S., Ryan, J. C., & Van Dolah, F. M. (2006). Microarray validation: factors influencing correlation between oligonucleotide microarrays and real-time PCR. *Biol Proced Online*, *8*, 175-193. https://doi.org/10.1251/bpo126

Mow, V. C., Wang, C. C., & Hung, C. T. (1999). The extracellular matrix, interstitial fluid and ions as a mechanical signal transducer in articular cartilage. *Osteoarthritis Cartilage*, *7*(1), 41-58. https://doi.org/10.1053/joca.1998.0161

Nakayama, N., Pothiawala, A., Lee, J. Y., Matthias, N., Umeda, K., Ang, B. K., Huard, J., Huang, Y., & Sun, D. (2020). Human pluripotent stem cell-derived chondroprogenitors for cartilage tissue engineering. *Cell Mol Life Sci*, *77*(13), 2543-2563. https://doi.org/10.1007/s00018-019-03445-2

Okamoto, T., Aoyama, T., Nakayama, T., Nakamata, T., Hosaka, T., Nishijo, K., Nakamura, T., Kiyono, T., & Toguchida, J. (2002). Clonal heterogeneity in differentiation potential of immortalized human mesenchymal stem cells. *Biochem Biophys Res Commun*, *295*(2), 354-361. https://www.ncbi.nlm.nih.gov/pubmed/12150956

Pchelintseva, E., & Djamgoz, M. B. A. (2018). Mesenchymal stem cell differentiation: Control by calcium-activated potassium channels. *J Cell Physiol*, *233*(5), 3755-3768. https://doi.org/10.1002/jcp.26120

Saeed, A., Francini, N., White, L., Dixon, J., Gould, T., Rashidi, H., Al Ghanami, R. C., Hruschka, V., Redl, H., Saunders, B. R., Alexander, C., & Shakesheff, K. M. (2015). A thermoresponsive and magnetic colloid for 3D cell expansion and reconfiguration. *Adv Mater*, *27*(4), 662-668. https://doi.org/10.1002/adma.201403626

Suzuki, Y., Yamamura, H., Imaizumi, Y., Clark, R. B., & Giles, W. R. (2020). K(+) and Ca(2+) Channels Regulate Ca(2+) Signaling in Chondrocytes: An Illustrated Review. *Cells*, *9*(7). https://doi.org/10.3390/cells9071577

Urban, J. P., Hall, A. C., & Gehl, K. A. (1993). Regulation of matrix synthesis rates by the ionic and osmotic environment of articular chondrocytes. *J Cell Physiol*, *154*(2), 262-270. https://doi.org/10.1002/jcp.1041540208

Vaeth, M., Yang, J., Yamashita, M., Zee, I., Eckstein, M., Knosp, C., Kaufmann, U., Karoly Jani, P., Lacruz, R. S., Flockerzi, V., Kacskovics, I., Prakriya, M., & Feske, S. (2017).

ORAI2 modulates store-operated calcium entry and T cell-mediated immunity. *Nat Commun*, *8*, 14714. https://doi.org/10.1038/ncomms14714

Wakle-Prabagaran, M., Lorca, R. A., Ma, X., Stamnes, S. J., Amazu, C., Hsiao, J. J., Karch, C. M., Hyrc, K. L., Wright, M. E., & England, S. K. (2016). BKCa channel regulates calcium oscillations induced by alpha-2-macroglobulin in human myometrial smooth muscle cells. *Proc Natl Acad Sci U S A*, *113*(16), E2335-2344. https://doi.org/10.1073/pnas.1516863113

Wilson, J. R., Duncan, N. A., Giles, W. R., & Clark, R. B. (2004). A voltage-dependent K+ current contributes to membrane potential of acutely isolated canine articular chondrocytes. *J Physiol*, *557*(Pt 1), 93-104. https://doi.org/10.1113/jphysiol.2003.058883

Zhang, Y. Y., Yue, J., Che, H., Sun, H. Y., Tse, H. F., & Li, G. R. (2014). BKCa and hEag1 channels regulate cell proliferation and differentiation in human bone marrow-derived mesenchymal stem cells. *J Cell Physiol*, *229*(2), 202-212. https://doi.org/10.1002/jcp.24435

Zhao, Y., Wei, H., Kong, G., Shim, W., & Zhang, G. (2013). Hydrogen sulfide augments the proliferation and survival of human induced pluripotent stem cell-derived mesenchymal stromal cells through inhibition of BKCa. *Cytotherapy*, *15*(11), 1395-1405. https://doi.org/10.1016/j.jcyt.2013.06.004

Figure legends

Figure 1. (A) Principal component analysis (PCA) showing transcriptomic differences between expression microarray data of both CPC and MSC cells ($N = 3$). Each sample group is represented by a sphere and is colour-coded to indicate the corresponding cell type category. There is a clear difference in the transcriptomic clustering between MSC and CPC samples. **(B)** Volcano plot showing differential expressed genes between CPC and MSC cells. The vertical axis (y-axis) corresponds to the log10 p-value < 0.05 and the horizontal axis (x-axis) displays the log2 fold change. Based on these parameters, the dots in the upper left and right areas represent differentially expressed genes with statistical significance.

Figure 2. Heatmaps and hierarchical clustering dendrograms for genes coding for **(A)** potassium channel subunits, **(B)** sodium channel subunits, **(C)** proteins involved in mediating

calcium homeostasis and other non-selective ion channels, and **(D)** acid sensitive cation channels and chloride channels. Results are expressed as fold change of gene expression of CPC *versus* MSC cells. The red colour represents upregulation, black colour indicates an unchanged expression, and blue colour represent downregulation of expression. The pattern and length of the branches in the dendrogram reflect the relatedness of the samples. Genes which were significantly up or down regulated in CPC *versus* MSC cells are highlighted in boldface; the red colour represents upregulation, and blue colour represents downregulation of expression. $N = 3$ biological replicates.

Figure 3. Transcript expression levels of selected genes coding for Ca^{2+} dependent potassium channel subunits as determined by RT-qPCR in CPC cells. Red bars represent upregulation, and blue bars represent downregulation of expression relative to MSCs, after being normalised to the reference gene *PPIA*. Representative data (average ± SEM; $N = 3$) out of 3 independent experiments (biological replicates) showing the same tendency of changes. Statistically significant (*$P < 0.05$; **$P < 0.01$) differences compared to MSCs are marked by asterisk(s).

Figure 4. Mitochondrial activity, as a measure of cell viability **(A)** and proliferation rate **(B)** were determined by MTT test and ^{3}H-thymidine incorporation assays, respectively, following pharmacological modulation of BK channel function in CPC *versus* MSC. Representative data (average ± SEM) out of 3 independent experiments ($N = 3$ biological replicates) showing the same tendency of changes (data are mean of $n = 8$ samples in each replicate). For each experimental group, data were normalized to that of the respective vehicle control (not shown individually). Statistically significant (*$P < 0.05$) differences compared to the vehicle control are marked by asterisk. **(C)** Osteochondrogenic marker gene expression after 1 μM paxilline treatment as determined by RT-qPCR in CPC cells after being normalised to PPIA.

Representative data (mean ± SEM; n = 3) out of 3 independent experiments (biological replicates) showing the same tendency of changes. Statistically significant (*$P < 0.05$) differences compared to control (DMSO) CPCs are marked by asterisk(s).

Figure 5. (A) Fibronectin-guided migration of CPCs in a Boyden chemotaxis chamber was significantly increased in the presence of 1 μM paxilline. Data shown are mean ± SEM; *$P <$ 0.05. $N = 3$ independent experiments. **(B)** The total length of movement, the maximum distance from the starting point, the average cell speed, and the maximum speed of the chondroprogenitor cells are depicted either without or with 1 μM paxilline treatment as determined during live-cell imaging. The total duration of live cell microscopy was 18 h; frame rate: 2/1 h; N = 3 independent experiments; 24–27 cells were analysed in each experiment. Total number of analysed cells: 77–80 cells/treatment group. Data are reported as mean ± SEM; *$P < 0.05$. **(C)** Representative wind-rose plots depict the total path of the cells. Each coloured line represents the total path of a single chondroprogenitor cell either without or with 1 μM paxilline treatment.

Figure 6. (A) Representative photomicrographs of CPC and MSC cell morphology prior to preparations for DEP measurements, showing typical mesenchymal cell morphology. Scale bar, 30 μm. **(B)** DEP parameters of CPCs and MSCs. The effective membrane capacitance (C_{Eff}), intracellular conductivity and specific membrane conductance (G_{Spec}) values were derived by fitting lines of best fit to DEP spectra and applying the 'single-shell model'. Membrane capacitance per cell was calculated by multiplying the capacitance values with the average surface area of the cells. Error bars denote the standard deviations (SD). Each experiment was repeated three times (N = 3). Asterisk denotes a statistically significant difference (*$P < 0.05$). **(C)** Examples of typical electrophysiological DEP (light intensity)

spectra of CPCs (n = 22) and MSCs (n = 14) produced using the DEP-microwell, together with a 'best-fit' model from which the dielectric properties were determined. Changes in light intensity in the region of interest detected over a 30 s exposure were plotted against frequency (between 1.6 kHz–20 MHz). The spectra are negative at low frequencies, where cells are repelled from the electrodes; at higher frequencies the spectra become positive, where cells are being attracted to the electrodes. The spectra gradually increase until a plateau stage is reached. At even higher frequencies, the spectra begin to decrease (mainly for CPCs).

Figure 7. Representative whole-cell currents of MSC and CPC cells. Resting membrane potential was held at –60 mV. Current elicited by voltage step depolarizations between –40 and +120 mV are shown in MSC (**A**) and CPC (**B**) cells under control conditions and during paxilline treatment (n = 27 for CPC and 7 for MSC). For both (**A**) and (**B**), I–V relationship of outward, paxillin-sensitive (full squares) and paxilline-insensitive (empty circles) currents in MSC (n = 7) and CPC (n = 27) cells are also shown. (**C**) Resting membrane potential values determined during patch clamp measurements (n = 22 for CPC and 8 for MSC). (**D**) Spontaneous calcium events in CPCs determined during live-cell Ca^{2+} imaging (n = 112 control *vs*. 83 paxilline-treated). Asterisks denote a statistically significant difference (***$P < 0.001$). Pax: paxilline

Tables

Table 1. Electrophysiological characteristics of CPC and MSC cells grown in standard monolayer cultures as determined by the DEP well chip and the single-shell model applied to the data. Values shown were averaged over 3 repeats of separate populations with ± SD given in brackets.

	CPC	*MSC*	*P-value*
Cell radius (μm)	9.6 (± 1.43)	11 (± 1.37)	<0.001
Effective membrane capacitance (mF/m^2)	12.84 (± 4.44)	11.29 (± 3.71)	0.298
Membrane capacitance per cell (pF)	14.86 (± 5.13)	17.16 (± 5.65)	0.231
Intracellular conductivity (S/m)	0.19 (± 0.06)	0.22 (± 0.06)	0.203
Specific membrane conductance (S/m^2)	827.48 (± 215.64)	623.15 (± 168.56)	0.006

Table 1. Electrophysiological characteristics of CPC and MSC cells grown in standard monolayer cultures as determined by the DEP well chip and the single-shell model applied to the data. Values shown were averaged over 3 repeats of separate populations with ± SD given in brackets.

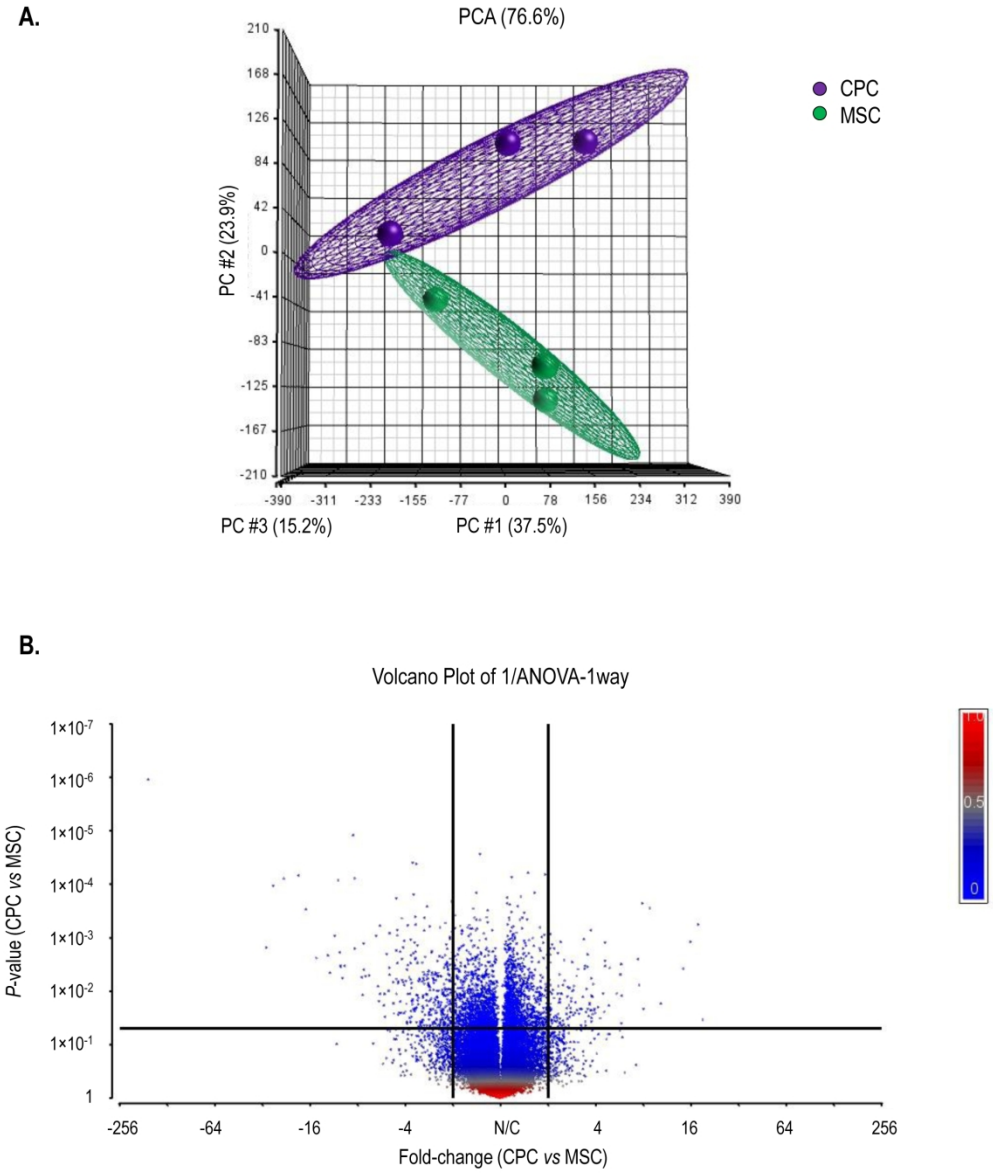

Figure 1. (A) Principal component analysis (PCA) showing transcriptomic differences between expression microarray data of both CPC and MSC cells (N = 3). Each sample group is represented by a sphere and is colour-coded to indicate the corresponding cell type category. There is a clear difference in the transcriptomic clustering between MSC and CPC samples. (B) Volcano plot showing differential expressed genes between CPC and MSC cells. The vertical axis (y-axis) corresponds to the log10 p-value < 0.05 and the horizontal axis (x-axis) displays the log2 fold change. Based on these parameters, the dots in the upper left and right areas represent differentially expressed genes with statistical significance.

187x224mm (300 x 300 DPI)

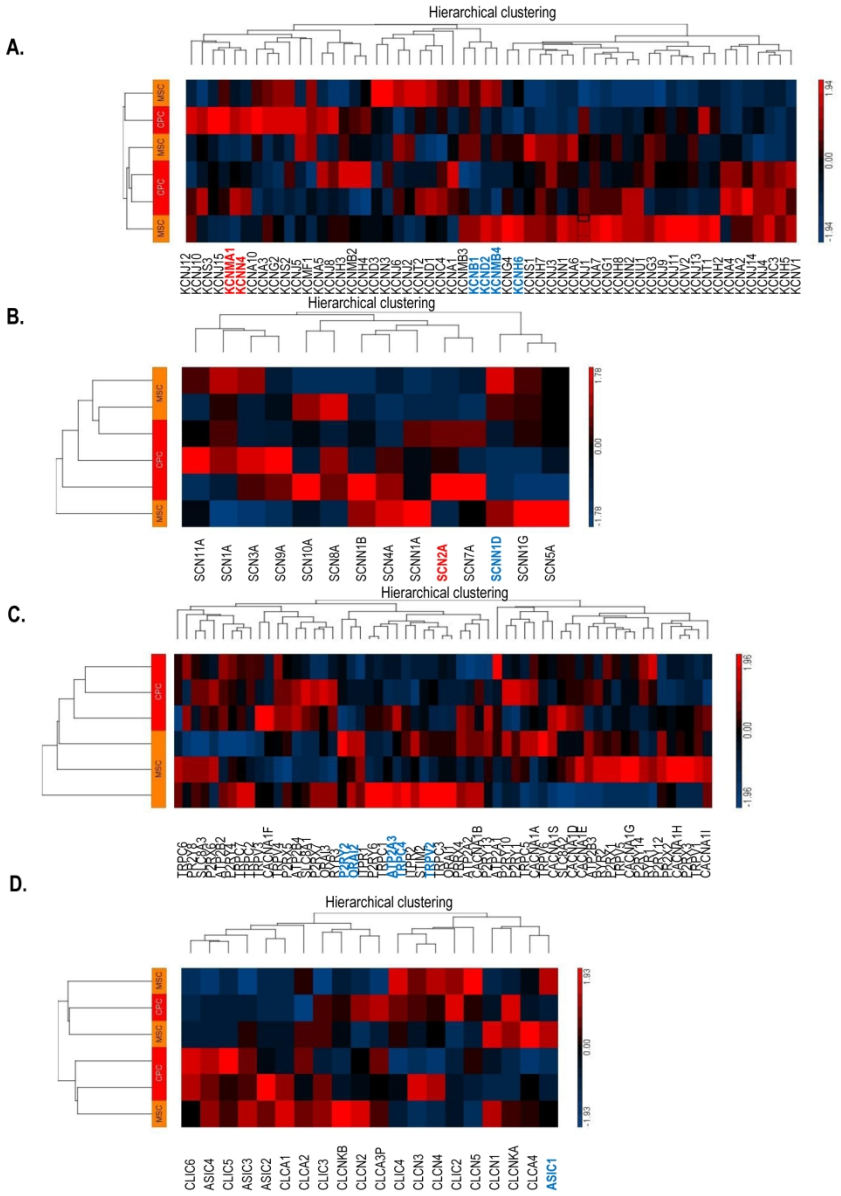

Figure 2. Heatmaps and hierarchical clustering dendrograms for genes coding for (A) potassium channel subunits, (B) sodium channel subunits, (C) proteins involved in mediating calcium homeostasis and other non-selective ion channels, and (D) acid sensitive cation channels and chloride channels. Results are expressed as fold change of gene expression of CPC versus MSC cells. The red colour represents upregulation, black colour indicates an unchanged expression, and blue colour represent downregulation of expression. The pattern and length of the branches in the dendrogram reflect the relatedness of the samples. Genes which were significantly up or down regulated in CPC versus MSC cells are highlighted in boldface; the red colour represents upregulation, and blue colour represents downregulation of expression. N = 3 biological replicates.

186x266mm (300 x 300 DPI)

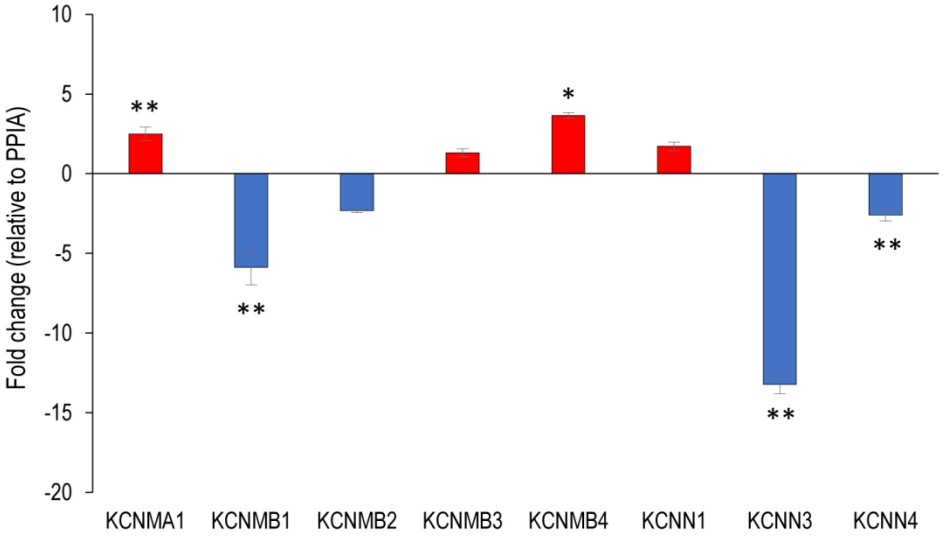

Figure 3. Transcript expression levels of selected genes coding for Ca2+ dependent potassium channel subunits as determined by RT-qPCR in CPC cells. Red bars represent upregulation, and blue bars represent downregulation of expression relative to MSCs, after being normalised to the reference gene PPIA. Representative data (average ± SEM; N = 3) out of 3 independent experiments (biological replicates) showing the same tendency of changes. Statistically significant (*P < 0.05; **P < 0.01) differences compared to MSCs are marked by asterisk(s).

135x80mm (300 x 300 DPI)

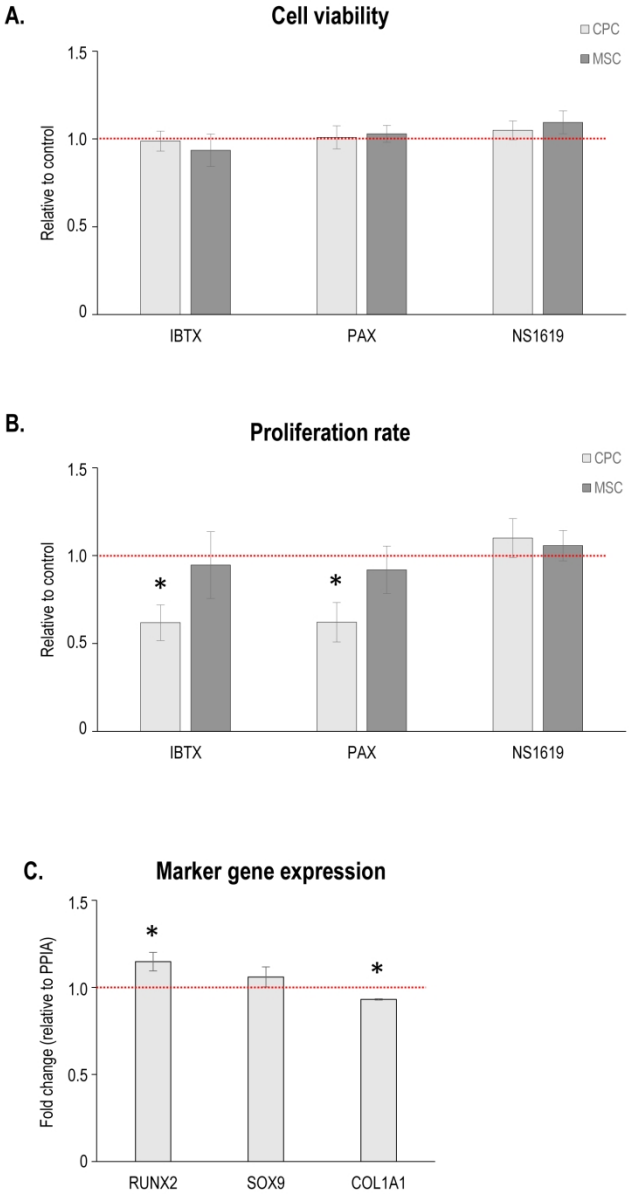

Figure 4. Mitochondrial activity, as a measure of cell viability (A) and proliferation rate (B) were determined by MTT test and 3H-thymidine incorporation assays, respectively, following pharmacological modulation of BK channel function in CPC versus MSC. Representative data (average ± SEM) out of 3 independent experiments (N = 3 biological replicates) showing the same tendency of changes (data are mean of n = 8 samples in each replicate). For each experimental group, data were normalized to that of the respective vehicle control (not shown individually). Statistically significant (*P < 0.05) differences compared to the vehicle control are marked by asterisk. (C) Osteochondrogenic marker gene expression after 1 μM paxilline treatment as determined by RT-qPCR in CPC cells after being normalised to PPIA. Representative data (mean ± SEM; n = 3) out of 3 independent experiments (biological replicates) showing the same tendency of changes. Statistically significant (*P < 0.05) differences compared to control (DMSO) CPCs are marked by asterisk(s).

137x241mm (300 x 300 DPI)

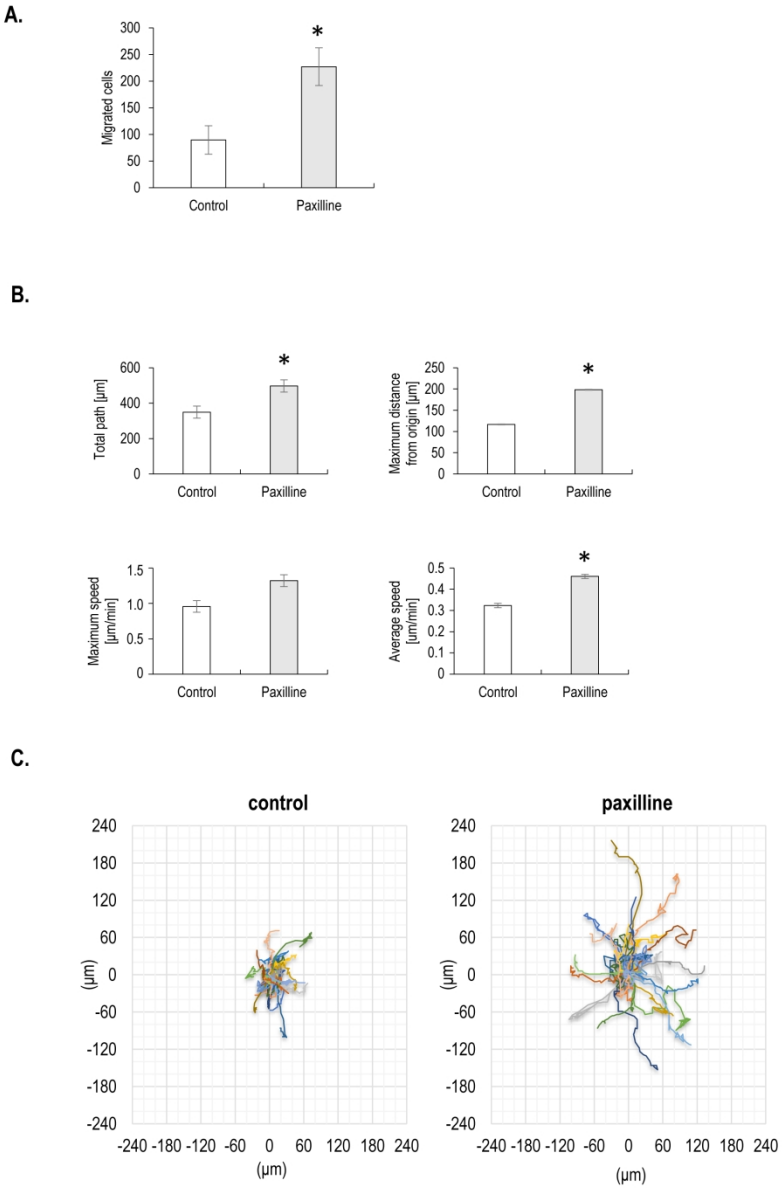

Figure 5. (A) Fibronectin-guided migration of CPCs in a Boyden chemotaxis chamber was significantly increased in the presence of 1 µM paxilline. Data shown are mean ± SEM; *P < 0.05. N = 3 independent experiments. (B) The total length of movement, the maximum distance from the starting point, the average cell speed, and the maximum speed of the chondroprogenitor cells are depicted either without or with 1 µM paxilline treatment as determined during live-cell imaging. The total duration of live cell microscopy was 18 h; frame rate: 2/1 h; N = 3 independent experiments; 24–27 cells were analysed in each experiment. Total number of analysed cells: 77–80 cells/treatment group. Data are reported as mean ± SEM; *P < 0.05. (C) Representative wind-rose plots depict the total path of the cells. Each coloured line represents the total path of a single chondroprogenitor cell either without or with 1 µM paxilline treatment.

175x257mm (300 x 300 DPI)

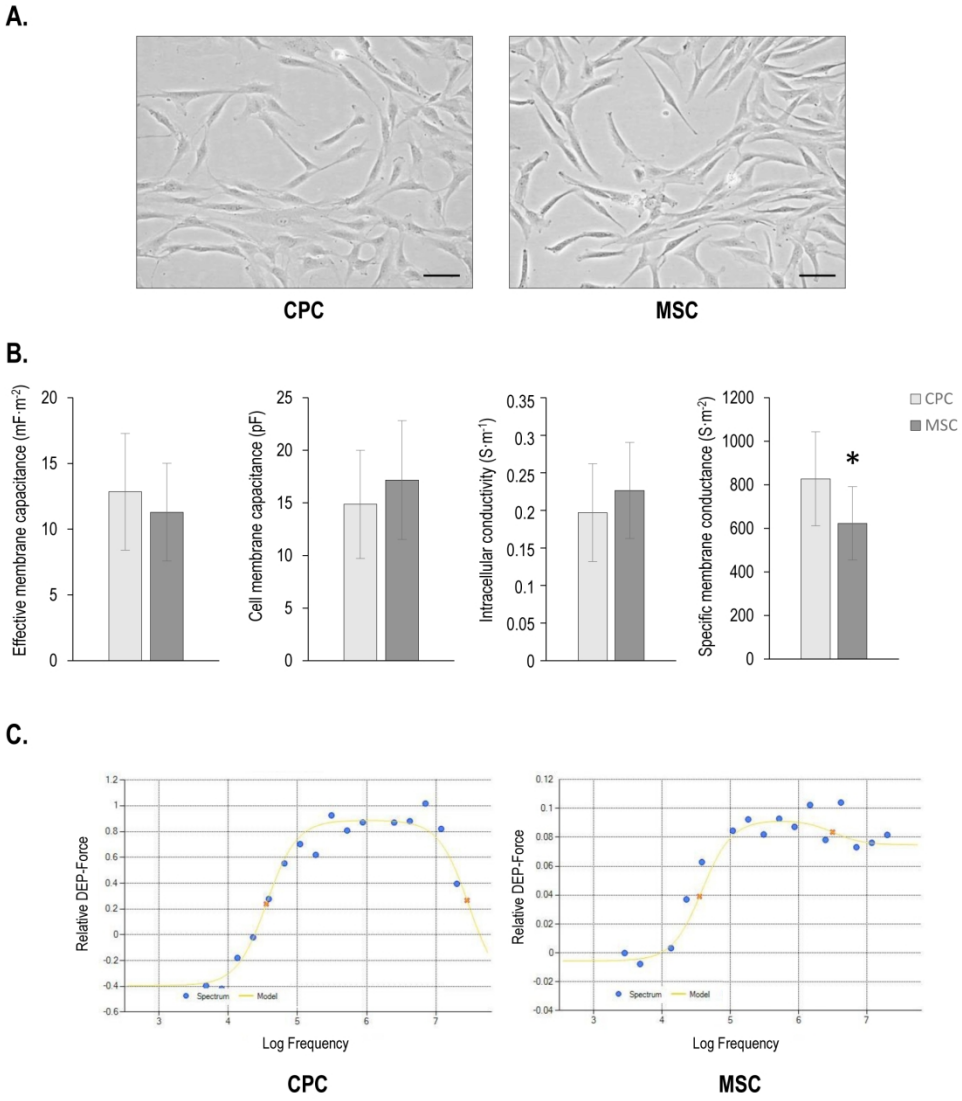

Figure 6. (A) Representative photomicrographs of CPC and MSC cell morphology prior to preparations for DEP measurements, showing typical mesenchymal cell morphology. Scale bar, 30 μm. (B) DEP parameters of CPCs and MSCs. The effective membrane capacitance (CEff), intracellular conductivity and specific membrane conductance (GSpec) values were derived by fitting lines of best fit to DEP spectra and applying the 'single-shell model'. Membrane capacitance per cell was calculated by multiplying the capacitance values with the average surface area of the cells. Error bars denote the standard deviations (SD). Each experiment was repeated three times (N = 3). Asterisk denotes a statistically significant difference (*P < 0.05). (C) Examples of typical electrophysiological DEP (light intensity) spectra of CPCs (n = 22) and MSCs (n = 14) produced using the DEP-microwell, together with a 'best-fit' model from which the dielectric properties were determined. Changes in light intensity in the region of interest detected over a 30 s exposure were plotted against frequency (between 1.6 kHz–20 MHz). The spectra are negative at low frequencies, where cells are repelled from the electrodes; at higher frequencies the spectra become positive, where cells are being attracted to the electrodes. The spectra gradually increase until a plateau stage is reached. At even higher frequencies, the spectra begin to decrease (mainly for CPCs).

178x200mm (300 x 300 DPI)

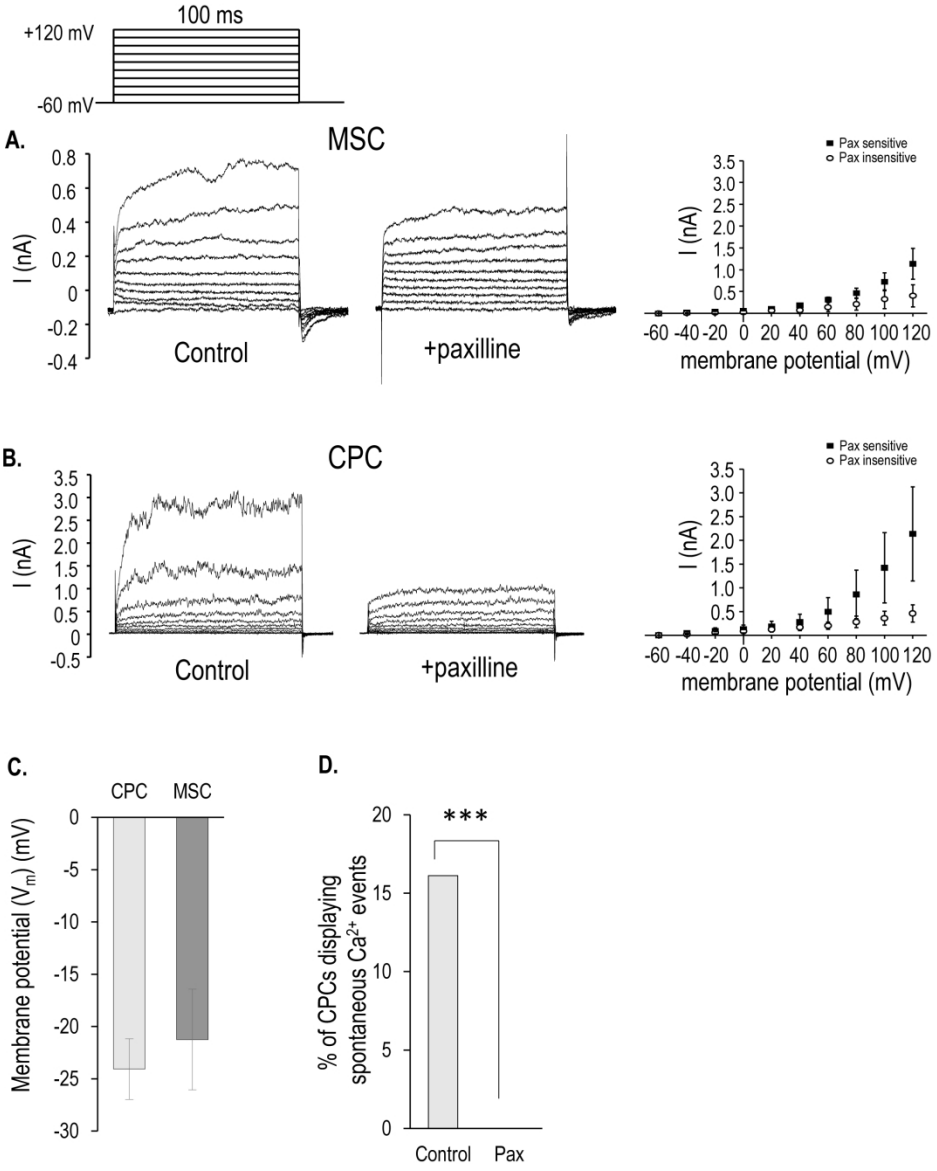

Figure 7. Representative whole-cell currents of MSC and CPC cells. Resting membrane potential was held at −60 mV. Current elicited by voltage step depolarizations between −40 and +120 mV are shown in MSC (A) and CPC (B) cells under control conditions and during paxilline treatment (n = 27 for CPC and 7 for MSC). For both (A) and (B), I–V relationship of outward, paxillin-sensitive (full squares) and paxilline-insensitive (empty circles) currents in MSC (n = 7) and CPC (n = 27) cells are also shown. (C) Resting membrane potential values determined during patch clamp measurements (n = 22 for CPC and 8 for MSC). (D) Spontaneous calcium events in CPCs determined during live-cell Ca2+ imaging (n = 112 control vs. 83 paxilline-treated). Asterisks denote a statistically significant difference (***P < 0.001). Pax: paxilline

188x238mm (300 x 300 DPI)